

Design of a High Altitude Long Endurance Solar Powered UAV Solar Powered Aerial Communicator (SPACOM)

A project present to
The Faculty of the Department of Aerospace Engineering
San Jose State University

in partial fulfillment of the requirements for the degree
Master of Science in Aerospace Engineering

By

Yaser Najafi

May 2011

approved by



Dr. Nikos Mourtos



Committee Members:

Dr. Nikos J. Mourtos, San Jose State University

Dr. Periklis Papadopoulos, San Jose State University

Mark Sidletsky, Pacific Scientific EMC

San Jose State University

The Undersigned Committee Approves

DESIGN OF A HIGH ALTITUDE LONG ENDURANCE SOLAR POWERED UAV
SPACOM (Solar Powered Aerial Communicator)

by

Yaser Najafi

APPROVED FOR THE DEPARTMENT OF MECHANICAL AND AEROSPACE
ENGINEERING

Dr. Nikos J. Mourtos, Committee Chair
San Jose State University



Dr. Periklis Papadopoulos, Committee Member
San Jose State University



Mark Sidletsky, Committee Member
Pacific Scientific EMC

Table of Contents

List of Figures.....	v
List of Tables.....	vii
List of Acronyms.....	viii
Acknowledgements.....	2
Abstract.....	3
1.0 Introduction.....	5
1.1 Unmanned Flight.....	5
1.2 Solar Powered UAVs.....	5
1.3 Military UAVs.....	11
1.4 Satellite Communications.....	14
1.5 SPUAV Need.....	15
1.6 Summary.....	15
2.0 Mission Specification.....	16
2.1 Mission Objective.....	16
2.2 Mission Requirements.....	16
2.3 Mission Profile.....	17
2.3.1 Flight Profile.....	17
3.0 Solar Energy.....	18
3.1 Solar Radiation.....	18
3.2 Solar Cell Selection.....	21
4.0 Rechargeable Batteries.....	22
5.0 Fuel Cells.....	23
6.0 Flight Theory.....	25
6.1 Aerodynamic Theory.....	25
7.0 Preliminary Sizing.....	28
7.1 Main Wing.....	28
7.2 Empennage.....	30
7.4 Configuration Selection.....	33
7.5 Fuselage.....	34
7.6 Drive train.....	35
7.7 Airfoil Selection.....	36
7.7.1 Wing Airfoil.....	36
7.7.2 Empennage Airfoil.....	43
8.0 Control Surface.....	47
8.1 Horizontal Stabilizer.....	47
8.2 Vertical Stabilizer.....	48
9.0 Landing Gear.....	49
10.0 Weight Analysis.....	51
10.1 Airframe Weight.....	51
10.2 Solar Cells.....	51
10.3 Fuel Cell.....	52
10.4 Payload.....	52
10.5 Gross Weight & Balance.....	52

11.0 Stability & Controls.....	55
11.1 Static Longitudinal Stability.....	55
11.2 Static Directional Stability.....	57
12.0 Performance.....	58
12.1 Power Performance.....	58
12.2 Take-off Performance.....	59
12.3 Flight Performance.....	60
12.3 Landing.....	64
12.4 Drag Polar.....	65
13.0 Conclusions.....	67
14.0 Recommendations / Lessons Learned.....	69
15.0 Design Summary.....	70
16.0 Reference List.....	71
Appendix A.....	70
Appendix B.....	74

List of Figures

Figure 1: Sunrise I [1].....	5
Figure 2: Solar Riser [1].....	6
Figure 3: AV/NASA HALE UAV Production Timeline [3].....	6
Figure 4: Pathfinder in Flight [7].....	7
Figure 5: Pathfinder Plus in Flight [7].....	8
Figure 6: Centurion in Flight [7].....	8
Figure 7: Helios in Flight [7].....	9
Figure 8: Helios HP03 High Dihedral [3].....	9
Figure 9: Helios HP03 Complete Structural Failure [3].....	10
Figure 10: Military UAV Flight Hours by Year [4].....	11
Figure 11: Curtis N-9 (1918) [9].....	11
Figure 12: DARPA AMBER UAV [10].....	12
Figure 13: Predator RQ-1 [10].....	12
Figure 14: Global Hawk RQ-4 Layout Specifications [11].....	13
Figure 15: Component Layout of Global Hawk [11].....	14
Figure 16: Flight Timeline.....	17
Figure 17: World Average Cost per Watt of Solar Cells [5].....	18
Figure 18: World Average Solar Cell Production [6].....	19
Figure 19: Atmospheric Effects on Solar Radiation [26].....	20
Figure 20: Advance in Solar Cell Technology [27].....	21
Figure 21: Fuel Cell Properties [28].....	23
Figure 22: Space Shuttle Fuel Cell [25].....	24
Figure 23: Basic Aerodynamic Forces [18].....	25
Figure 24: Air Temperature vs. Altitude [19].....	26
Figure 25: Wind Speed vs. Altitude [20].....	27
Figure 26: Flying Wing Configuration.....	33
Figure 27: Conventional Configuration.....	33
Figure 28: Twin Boom Configuration.....	34
Figure 29: BLDC Motor Speed vs Torque Characteristics [12].....	35
Figure 30: Selig S1223 Size Characteristics [13].....	37
Figure 31: Liebeck LA2573A Size Characteristics [13].....	37
Figure 32: Wortmann FX 74-CL5-140 Size Characteristics [13].....	37
Figure 33: Reynolds Number over Chord of Wing.....	39
Figure 34: Reynolds Number Range Legend.....	40
Figure 35: FX 74-CL5-140 C_l vs C_d	41
Figure 36: FX 74-CL5-140 C_l vs AoA	41
Figure 37: FX 74-CL5-140 C_m vs AoA	42
Figure 38: FX 74-CL5-140 C_l/C_d vs AoA	42
Figure 39: NACA 0008 Size Characteristics [13].....	43
Figure 40: Reynolds Number Range Legend.....	44
Figure 41: NACA 0008 C_l vs C_d	44
Figure 42: NACA 0008 C_l vs AoA	45

Figure 43: NACA 0008 C_m vs AoA	45
Figure 44: NACA 0008 C_l/C_d vs AoA	46
Figure 45: Horizontal stabilizer Sizing.....	47
Figure 46: Vertical Stabilizer Sizing.....	48
Figure 47: Landing Gear.....	49
Figure 48: Main Landing Gear Layout.....	50
Figure 49: Breakaway Landing Gear Layout.....	50
Figure 50: SPACOM Weight & Balance.....	53
Figure 51: Longitudinal X-Plot.....	56
Figure 52: Directional X-Plot.....	57
Figure 53: Power Breakdown during Flight.....	58
Figure 54: Climb Rate with Increasing Altitude.....	61
Figure 55: Power with Respect to Altitude.....	62
Figure 56: Power Required at Sea Level.....	62
Figure 57: Power Required at 40,000 ft.....	63
Figure 58: Power Required at 65,000 ft.....	63
Figure 59: Descent Rate with Various Angles.....	64
Figure 60: C_d vs C_L	65
Figure 61: L/D vs C_L	65
Figure 62: Final Design.....	74
Figure 63: Initial Design with Low Gear.....	75
Figure 64: Landing Gear.....	75
Figure 65: Tail Configuration.....	76

List of Tables

Table 1: Solar HALE UAV Technical Comparison [7], [8].....	10
Table 2: Solar Radiation per Month of Year [2].....	20
Table 3: Advantage & Disadvantages of Various Battery Types.....	22
Table 4: Atmospheric Properties [17].....	26
Table 5: Wind Speed at Max. & Min. Altitudes.....	27
Table 6: Wing Geometry Results.....	30
Table 7: Empennage Geometry Results.....	31
Table 8: Horizontal Tail Volume Coefficient Variables.....	32
Table 9: Vertical Tail Volume Coefficient Variables.....	32
Table 10: Airfoil Aerodynamic Comparison [13].....	38
Table 11: Reynolds Number over Wing with Respect to Altitude.....	39
Table 12: NACA 0008 Characteristics [13].....	43
Table 13: Elevator Sizing.....	47
Table 14: Rudder Sizing.....	48
Table 15: Weight Estimate Breakdown.....	52
Table 16: Sub-System Distance Moment.....	54
Table 17: Mean Aerodynamic Chord Properties.....	55
Table 18: Stall Speed vs. Altitude.....	60
Table 19: Power Requirements with Altitude.....	63
Table 20: Wetted Area.....	65
Table 21: Raw Data with Respect to Altitude.....	70

List of Acronyms

SPACOM	Solar Powered Aerial Communicator
UAV	Unmanned Aerial Vehicle
RPV	Remote Piloted Vehicle
SPUAV	Solar Powered Unmanned Aerial Vehicle
HALE	High Altitude Long Endurance
AV	AeroVironment
NASA	National Aeronautics & Space Administration
PV	Photovoltaic
MW	Megawatt
USMS	United States Military Services
DARPA	Defense Advanced Research Project Agency
TUAV	Tactical Unmanned Aerial Vehicle
HAE	High Altitude Endurance
AC	Aerodynamic Center
NP	Neutral Point
C_L	Lift Coefficient
C_d	Drag Coefficient
C_m	Moment Coefficient
AoA	Angle of Attack
S_w	Wing Surface Area
S_t	Tail Surface Area
S_h	Horizontal Tail Surface Area
S_v	Vertical Tail Surface Area
V_∞	Free Stream Velocity
V	Velocity
P	Power
P_R	Power Required
P_A	Power Available
L	Lift
D	Drag
T_R	Thrust Required
R/C	Rate of Climb
L/D	Lift-Drag Ratio
V_v	Vertical Tail Volume Coefficient
V_h	Horizontal Tail Volume Coefficient
ρ	Density
μ	Kinematic Viscosity
c_0	Root Chord
c_t	Tip Chord
\bar{X}_{ac_w}	Mean Aerodynamic Center Distance of Wing
$C_{L_{ah}}$	Lift Coefficient Slope of Horizontal Tail
$\frac{\partial \epsilon}{\partial \alpha}$	Down Wash Angle Slope with respect to AoA
\bar{X}_{ac_h}	Distance of Mean Aerodynamic Center of Horizontal Tail to Wing

San Jose State University

The Undersigned Committee Approves

DESIGN OF A HIGH ALTITUDE LONG ENDURANCE SOLAR POWERED UAV
SPACOM (Solar Powered Aerial Communicator)

by

Yaser Najafi

APPROVED FOR THE DEPARTMENT OF MECHANICAL AND AEROSPACE
ENGINEERING

Dr. Nikos J. Mourtos, Committee Chair
San Jose State University

Date

Dr. Periklis Papadopoulos, Committee Member
San Jose State University

Date



Mark Sidletsky, Committee Member
Pacific Scientific EMC

5/19/2001
Date

Acknowledgements

I would like to take the opportunity to thank all those who took the time to help me through my long and challenging educational career at San Jose State University.

Firstly, I want to thank Dr. Nikos J. Mourtos and Dr. Periklis Papadopoulos for being there not only through my graduate studies, but my undergraduate studies as well; without your guidance and support none of this would be possible.

Secondly, I would like to thank Mark Sidletsky for breaking away from our chaotic work environment and taking the time to educate me throughout this study. Without your help, I think I wouldn't have kept my sanity.

Finally, I would like to thank my family and my close friends for being there, without your encouragement I would not be where I am today.

“...Impossible is nothing.” –Muhammad Ali.

Abstract

This research shall investigate the design and component selection to be used for a solar powered HALE UAV to be implemented as a communication beacon to minimize radio wave propagation. A better understanding of the design and the most optimal configuration selection can be determined by performing a historical analysis on previous UAVs, as well as solar powered UAVs. Due to the long endurance and the high altitudes it is feasible to select design specifications similar to the *Helios* solar powered UAV, which is achieved a maximum altitude of 96,000 feet. The overall configuration was designed around the failure modes which lead *Helios* to crash. Although the SPACOM is over designed, with the correct airfoil selection, wing configuration, and power systems it is possible for a UAV to stay aloft for 30+ days.

PAGE INTENTIONALLY LEFT BLANK

1.0 Introduction

1.1 Unmanned Flight

Since WWI there has been an unprecedented need to develop tactical Unmanned Aerial Vehicles (UAVs). The earliest known UAV or Remote Piloted Vehicle (RPV) “Aerial Target” was developed in 1916, by A.M Low [2]. With the advancement of technology, UAVs have become a dominating component not only combat flight but in commercial flight as well. UAVs have become multifunction devices used for:

- Remote Sensing
- Material Transport
- Scientific Research
- Tactical Military Attacks
- Search & Rescue

1.2 Solar Powered UAVs

Within the past 30 years there has been a great effort set on designing and successfully manufacturing a UAV which only relays on reusable energy. This idea came to life when Astro Flight successfully built the first Solar Powered UAV (SPUAV), Sunrise I (Figure 1) [1]. The success of Sunrise I became proof that a UAV can be built to be powered only solar energy for High Altitude Long Endurance (HALE) flight.

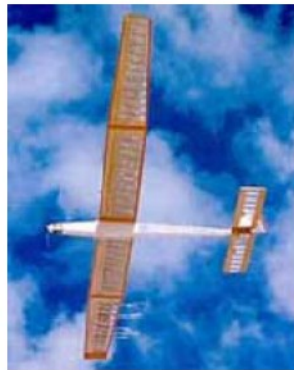


Figure 1: Sunrise I [1]

The next leap in SPUAV technology came in 1979 when Ultralight Flying Machines built the Solar Riser (Figure 2) [1]. The “Riser” did not have the capability of flight solely on solar power, but used solar energy to charge the onboard batteries, which powered the 3.5 hp electric motor.



Figure 2: Solar Riser [1]

Some of the most current HALE UAVs have been developed by AeroVironment (AV) with the assistance of NASA. The following (Figure 3) aircraft have been designed and have had proto-types built:

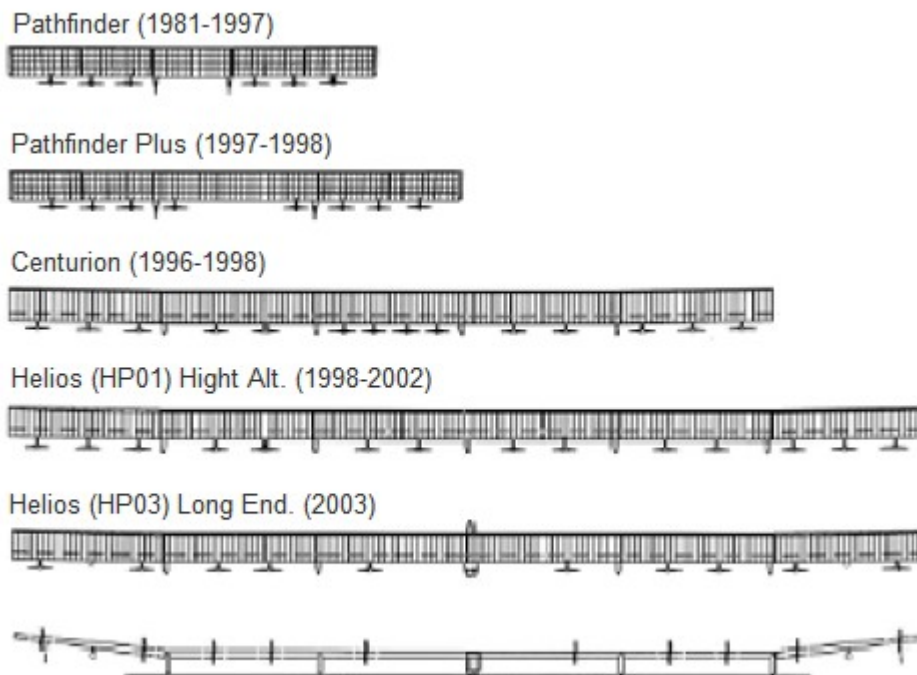


Figure 3: AV/NASA HALE UAV Production Timeline [3]

Thin-film solar cells have become vital for the endurance of HALE UAVs within the past decade. The major design aspect of a HALE UAV would be its ceiling altitude; it is vital for a HALE UAV to climb to a higher altitude to take advantage of the high amounts of solar radiation. This will also allow the HALE UAV more time to descend during night-time flight (if needed).

To date there have been several efforts on manufacturing a HALE UAV. The most prominent ones are shown in Table 1. AeroVironment (AV) with the assistance of NASA has become one of the most profound organizations to successfully build a HALE SPUAV, which happens to hold the world altitude record. In 1995, AV manufactured the Pathfinder (Figure 4) was able to reach a maximum altitude of 50,000 feet. Pathfinder was powered by six (6) electric motors, and had a power output of approximately 7,500 watts [7].



Figure 4: Pathfinder in Flight [7]

In 1997, the more improved Pathfinder Plus (Figure 5) was able to reach a service ceiling of 80,000 feet. The improvements included a larger wing span for better stability, and an addition of two extra electric motors, four total.



Figure 5: Pathfinder Plus in Flight [7]

The next installment was the Centurion (Figure 6), which was originally designed to be able reach an altitude of 100,000 feet; although due to budget cuts the program was modified, and the Helios program was started [7].



Figure 6: Centurion in Flight [7]

Helios (Figure 7) was able to reach approximately 96,863 feet, which is the current world record holder. Helios was a major improvement from its predecessors, in which it was the first to implement an alternate fuel cell in addition to the rechargeable batteries. The fuel cell which was primarily used for night time flight, allowed the UAV to extend its endurance from days to weeks. The Helios program came to a halt when it encountered extreme high winds during flight, which caused excessive natural dihedral (Figure 8, Figure 9) which resulted in a catastrophic crash into the Pacific Ocean in 2003 [3].



Figure 7: Helios in Flight [7]



Figure 8: Helios HP03 High Dihedral [3]



Figure 9: Helios HP03 Complete Structural Failure [3]

The Zephyr which is manufactured by a UK based company, Qinetiq, was extremely light weight; the UAVs were able to achieve continuous flight for 14 days and 21 minutes reaching a maximum altitude of approximately 70,000 feet. Zephyr was able to achieve its range and endurance due the implementation of thin-film solar cells, which improved the UAVs power-to-weight ratio. As shown in Table 1, Zephyr is the smallest of all the comparative designs.

Table 1: Solar HALE UAV Technical Comparison [7], [8]

UAV	Span (ft)	Chord (ft)	Length (ft)	Area (ft ²)	Weight (lb.)	Motors	Alt. (ft)*
Zephyr	~60	~7	~9	~570	~70	2	60,000+
Pathfinder	~100	8	12	~800	~560	6	50,000
Pathfinder Plus	121	8	11	968	700	8	80,000
Centurion	206	8	12	1,648	~1,800	14	100,000
Helios	247	8	12	~2,000	~2,000	14	100,000+

**Altitude based on designed ability, not actual altitude reached. UAV may or may have not reached designed altitude.*

1.3 Military UAVs

Currently there are approximately 10,000+ UAVs in service by the United States Military Services (USMS) [4]; there applications range similar to that as specified in the previous section.

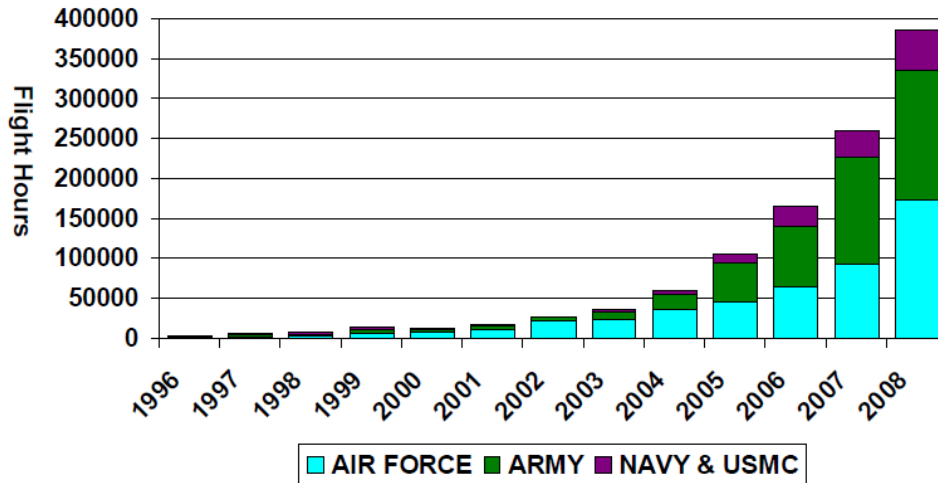


Figure 10: Military UAV Flight Hours by Year [4]

Use of UAVs for the USMS has been around since World War I; the earliest known UAV was the Curtiss N-9 used by the Navy. The N-9 (Figure 11) was able to carry a ~300 lb. payload (bomb) approximately 50 miles [9].



Figure 11: Curtiss N-9 (1918) [9]

The modern military UAV has become more of a dominant aerial vehicle due its advancement in aerodynamic maneuverability and its durability. These UAVs are usually sent on missions that may be too dangerous for military personnel.

Due to an increase in demand for the safety of the war fighter, there has been great emphasis on designing and developing long endurance UAVs. This type of UAV shall be able to give detection, tracking, observational, and communicational support to ground troops.

Currently, there are several high altitude UAVs used by the military. DARPA's AMBER program (Figure 12) was a medium-altitude UAV which was used during *Desert Storm*. The AMBER program lead to an evolution of Tactical UAVs (TUAVs), which are currently in use today; the Predator (Figure 13) is equipped with a 115 hp motor which can fly to a service ceiling of ~25,000 feet and can stay aloft for approximately 24 hours (unarmed) and approximately 16 hours (armed) [10].



Figure 12: DARPA AMBER UAV [10]



Figure 13: Predator RQ-1 [10]

The most current TUAV is Northrop Grumman's Global Hawk (Figure 14, Figure 15), which has evolved from the AMBER and Predator programs. The Global Hawk RQ-4,

which went into full scale production in 2001 cruises at ~400 mph and reaches a service ceiling of ~65,000 feet. Its high altitude capability gives the Global Hawk extreme aerial dominance in intelligence, surveillance and reconnaissance for ground forces [10].



Wingspan	116.2 ft
Length	44.4 ft
Height	14.6 ft
Takeoff Weight	26,750 lbs
Max Altitude	65,000 ft
Radar Capabilities	SATCOM data link, Dual Band COL LOS, UHF Command & Control, ATC Voice, Radar, ISAR, Electro-Optical, Infrared

Figure 14: Global Hawk RQ-4 Layout Specifications [11]

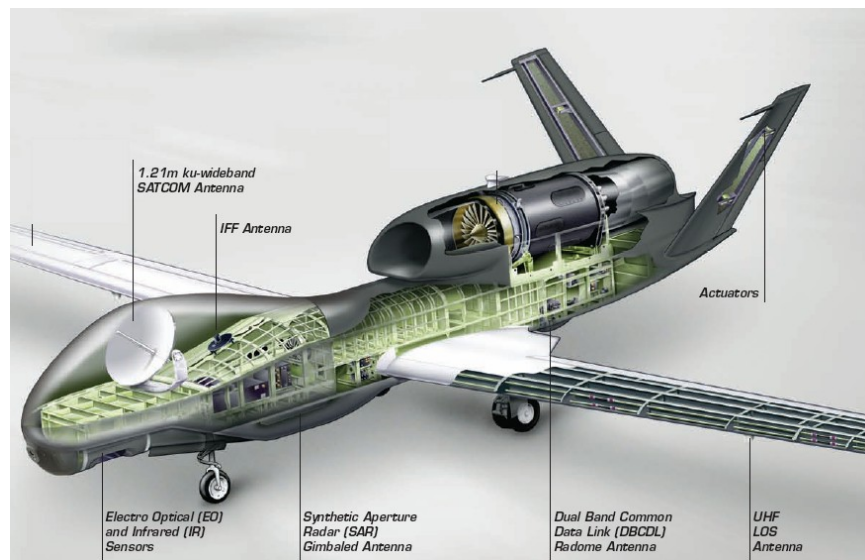


Figure 15: Component Layout of Global Hawk [11]

1.4 Satellite Communications

Currently the main sources of communication beacons are orbital satellites; the amount of satellites placed into orbit within last ten years has increase substantially. The advantages of a satellite are:

- Coverage area exceeds that of an aircraft.
- Transmission cost is independent of its distance from the ground.
- Satellite-to-satellite communication is extremely precise.
- Higher bandwidths are available.

However, there are many disadvantages with satellites as well, which are:

- Launching to orbit can be extremely costly.
- Bandwidth gradually increases in use over time.
- There is a larger propagation, with respect to data transmission.

1.5 SPUAV Need

Communication is a vital aspect in today's society, especially on the battlefield. A geosynchronous orbiting satellite requires an orbiting altitude of approximately 23,000 miles, and can be very costly. While, low altitude (military) satellites pass their intended focus area quickly, leaving ground support a small working window. If a HALE SPUAV were to be implemented to be able to stay in a single location it would dramatically increase the communication resolution.

Currently the Defense Advanced Research Projects Agency's (DARPA) Vulture program is based upon designing a HALE SPUAV which can stay aloft for five years to be used as a communications satellite. The UAV shall be completely autonomous and fully sustainable, with respect to energy. In order to achieve success all design aspects from most if not all previous UAVs must be taken into consideration; with the implementation of solar energy it will not require for the UAV to return for refueling or recharging.

1.6 Summary

In this chapter we introduced the most recent HALE UAVs. We discussed how they differ from one another and their accomplishments. We also introduced the history of medium-ranged UAVs for military purposes, and how they have become a dominant intelligence aircrafts. However, in order for a military UAV to have complete dominance of the sky, it must have the endurance abilities of a solar HALE UAV.

2.0 Mission Specification

2.1 Mission Objective

This research is to extend efforts on designing and developing a HALE UAV using an alternative fuel source. This research shall be done in conjunction with the current DARPA Vulture & Boeing Phantom Eye programs; both of which may potentially benefit the DoD, and any other government organization. UAVs can play a major role in other applications, such as, agriculture monitoring, wildfire surveillance, and border patrol. However, this research shall only focus the design HALE SPUAV.

2.2 Mission Requirements

The requirements of the HALE SPUAV shall be (but not limited to) the following:

- Stay aloft for 720 Hours (30 days) minimum (following take-off).
- Reach a maximum altitude of 65,000 feet (during 30 day flight).
- Reach a minimum altitude of 40,000 feet (during 30 day flight).
- Self sustainable by reusable energy source (during 30 day flight).
- Provide autonomous flight (take-off and land not a requirement).

2.3 Mission Profile

2.3.1 Flight Profile

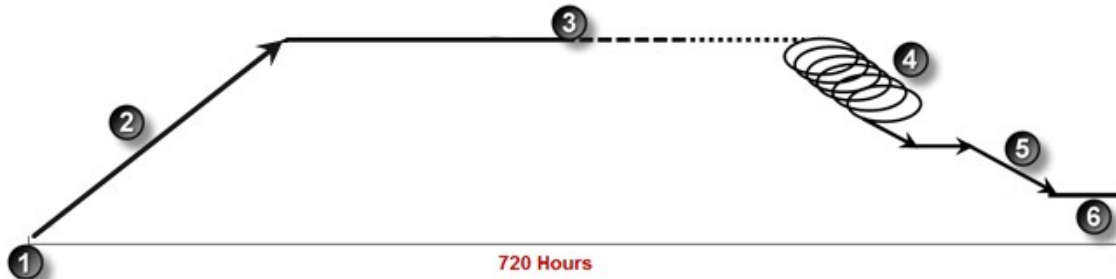


Figure 16: Flight Timeline

The flight time line as shown in Figure 16 shall be as follows:

1. Take-off.
2. Climb to maximum altitude.
3. Daytime / Night-time level flight.
4. Loitering descent.
5. Level flight / final descent.
6. Land.

3.0 Solar Energy

3.1 Solar Radiation

Solar radiation is radiation emitted energy by the sun onto a given surface, such as the Earth. Solar energy has been harnessed since ancient times to start fires, boil water, and even cook food. It was not until 1839 when French Physicist Alexander-Edmond Becquerel discovered the Photovoltaic Effect, which allowed solar energy to be converted into electrical energy. In 1883 Charles Fritts coated Selenium semiconductor with an extremely thin layer of gold to form the first solar cell, which was only 1% efficient [2].

Almost one hundred years later, the first silicon photovoltaic (PV) solar cell was created in 1954, which was approximately 4% efficient. Today, efficiencies can range from 18% - 40%; as the performance of solar cells increased, prices decreased. As depicted in Figure 17, the average cost per watt for an average PV solar cell has dramatically decreased throughout the years.

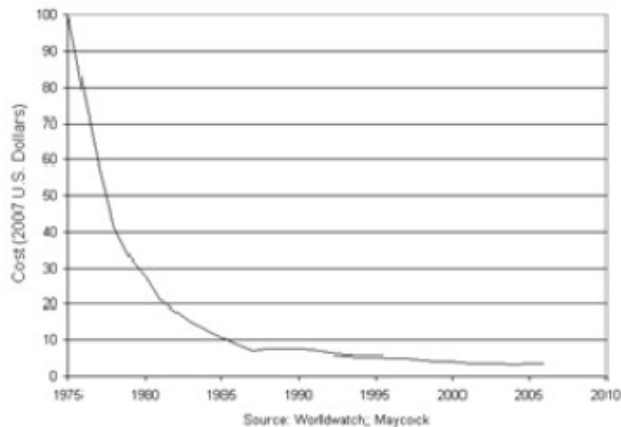


Figure 17: World Average Cost per Watt of Solar Cells [5]

The price drop was a direct result of the increase of solar cell production. Figure 18 below, shows a spike in PV solar cells per mega-watt (MW) at the beginning of the 21st Century.

The increase in production may have been a result of:

- Renewable energy endeavors
- Rising fossil fuel costs
- Environmental concerns

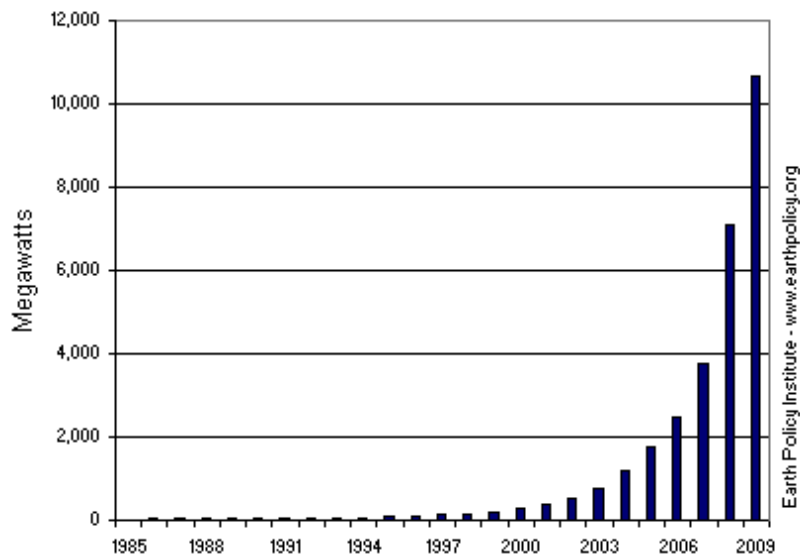


Figure 18: World Average Solar Cell Production [6]

The average amount of solar radiation (I_0) received at the edge of the Earth's atmosphere (at air mass 0, $AM\ 0$) is approximately $125.8\ \text{W}/\text{ft}^2$. Since the Sun-Earth orbit is elliptical the value of I_0 varies throughout the year, as shown below.

Table 2: Solar Radiation per Month of Year [2]

Month	Radiation* (W/ft ²)
Jan	129.97
Feb	129.50
Mar	128.11
Apr	125.79
May	123.83
Jun	121.88
Jul	121.51
Aug	121.88
Sep	123.46
Oct	125.41
Nov	127.55
Dec	129.32

**Values are dependent of location on the earth.*

The amount of actual amount of solar radiation over a specific region may be reduced to approximately 50% due to our atmosphere. The actual amount of solar energy which reaches the surface of the earth exceeds the total energy consumption [26]. Figure 19 below shows the solar radiation spectrum between *AM 0* (yellow curve) and *AM 1.5* (red curve). The primarily cause of the loss of power across the spectrum is absorption and reflection, as well as scattering due to water vapor and carbon dioxide in our atmosphere.

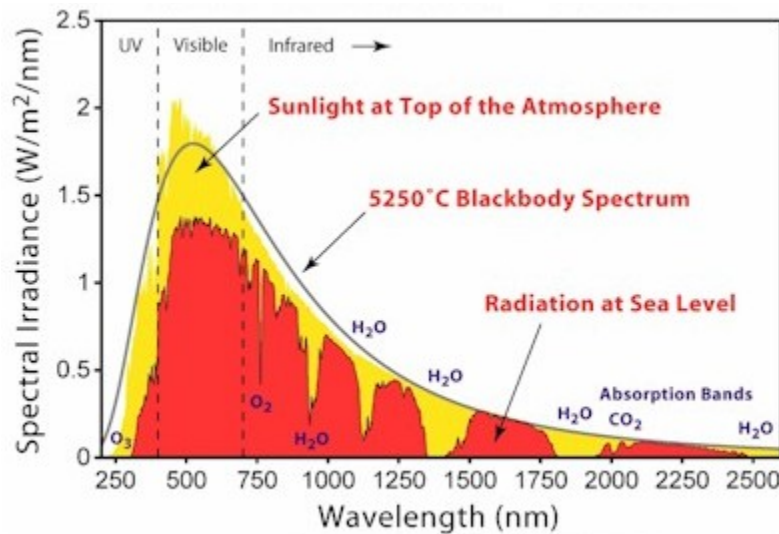


Figure 19: Atmospheric Effects on Solar Radiation [26]

3.2 Solar Cell Selection

There are various types of solar cells, made usually from semiconductor materials. The most common material is Silicon, which can also be the most expensive. Today with the advancing solar technology there is a wide variety of solar cells which are also light weight and more efficient. Figure 20 shows various solar cell types with respect to efficiency within the last 30 years.

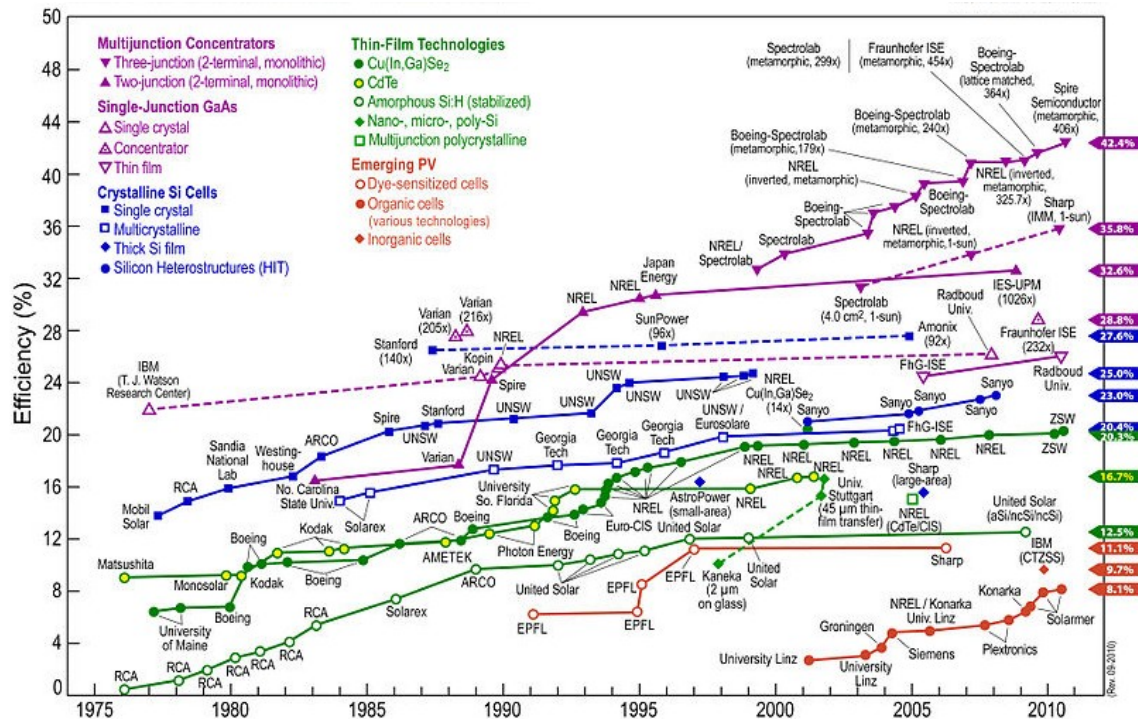


Figure 20: Advance in Solar Cell Technology [27]

As shown in Figure 20, the current solar cells made today can be up to 45% efficient. These types of solar cells are usually multi-junction solar cells; meaning they contain a single junction stacked over one other. The primary applications of high efficient solar cells are generally used for spacecraft applications.

For the purpose of this project the *Spectrolab NeXt Triple Junction (XTJ)* solar cell shall be chosen. The *XTJ* solar cells are approximately 29.5% efficient and are significantly lighter than other solar cells with similar efficiencies.

4.0 Rechargeable Batteries

The energy collected from the solar cells during day time hours may be stored within the on-board batteries to be used for night flight. Since the batteries used are critical, an analysis of various battery types was conducted, and is shown in Table 3. The types of batteries taken under consideration are: Lead-Acid, Lithium-Ion, Nickel-Cadmium, and Lithium-Polymer; all of which are capable of being fully recharged.

Table 3: Advantage & Disadvantages of Various Battery Types

Type	Advantage	Disadvantage
Lead-Acid	<ul style="list-style-type: none"> -Reliable and have been used for 100+ yrs. -Large amounts of technical data available. 	<ul style="list-style-type: none"> -Performance decreases as temperature increases. -Large in size (bulky).
Lithium-Ion	<ul style="list-style-type: none"> -Wide variety of shapes. -Lighter than most common batteries. -High open circuit voltage. 	<ul style="list-style-type: none"> -Charging time diminishes over time (high current usage). -High charge levels and high temperatures decrease capacity. -Loss rate varies by temperature.
Nickel-Cadmium	<ul style="list-style-type: none"> -Higher deep discharge. -Higher energy density (compared to Lead-Acid). -Voltage declines slower during discharge. 	<ul style="list-style-type: none"> -Higher cost (relative). -Pose charging problems during variance in temperature.
Lithium-Polymer	<ul style="list-style-type: none"> -Similar to Li-Ion. -Uses a polymer gel electrolyte. -More stable and robust casing. -Higher energy density. 	Similar to Li-Ion.

Since rechargeable battery technology has not advanced quickly enough in recent years, the energy density can be relatively low; also they can be extremely heavy. For the purpose of conserving weight, batteries will not be used in this study.

5.0 Fuel Cells

A fuel cell is similar to conventional rechargeable batteries; however the energy density is much higher, this is due to its ability to generate electrical energy from chemical energy. The space shuttle uses fuel cells as its primary power plant to generate all the electrical energy from launch through landing [25].

There are various types of fuel cells, however they are all made of three major components:

- Anode
- Cathode
- Electrolyte

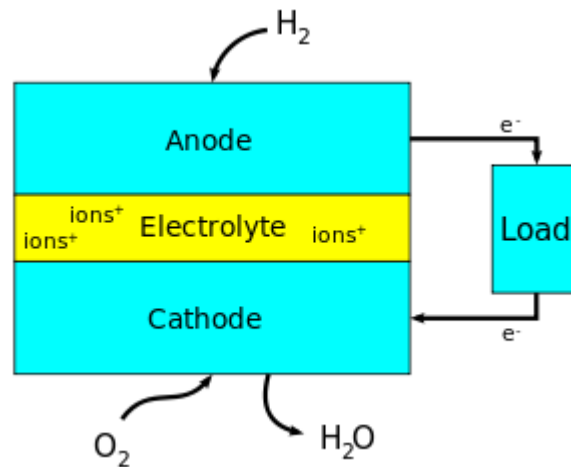


Figure 21: Fuel Cell Properties [28]

Figure 21 shows the basic process of electrical power generation by a fuel cell. When the fuel (usually Hydrogen) enters the anode it becomes a positively charged ion and a negatively charged electron. The electrolyte is designed so that the ions produced can pass directly through it, but the electrons cannot. The trapped electrons pass through an electrical system and in result create electrical energy. Once the ions pass the electrolyte and enter the cathode they are met with a third chemical (usually Oxygen) and create water (H_2O) or carbon dioxide (CO_2) as an emission.

Fuel cells of this type will dramatically play a major role in the overall weight of the SPACOM. A typical fuel cell system can be almost 25% - 50% lighter than a battery system [25]. Previous research has shown that the energy density of a standard $H_2 - O_2$ fuel cell can range between 0.450 – 0.650 kWh/kg [29]. The space shuttle uses three $H_2 - O_2$ fuel cells, which weigh approximately 150 lbs each; which generate 7kW of continuous power, and 12kW peak. For this matter the SPACOM shall implement three fuel cells similar to that of the space shuttle, as shown in Figure 22.

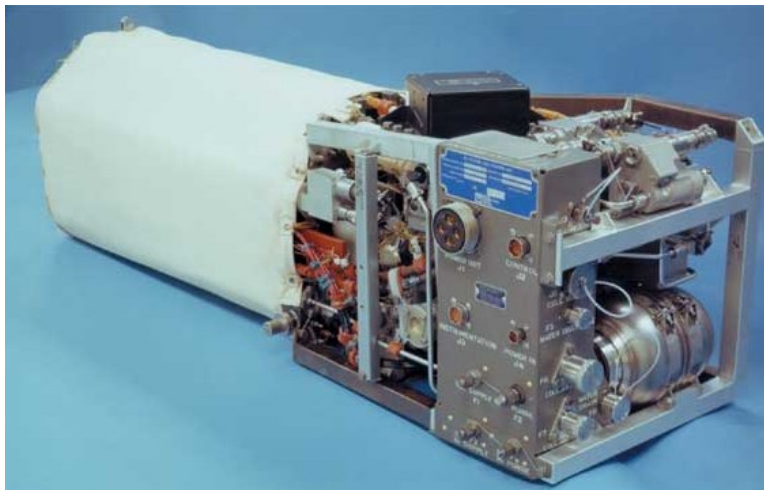


Figure 22: Space Shuttle Fuel Cell [25]

6.0 Flight Theory

6.1 Aerodynamic Theory

The SPACOM must meet the same aerodynamic principles as any conventional aircraft. Figure 23 below shows a basic free body diagram of the forces exerted onto an aircraft during flight. For level equilibrium flight it can be assumed that:

$$W = L \text{ And } T = D$$

(1)

Respectively the lift and drag can be expressed by,

$$L = \frac{1}{2} \rho V^2 S C_L$$

(2)

$$D = \frac{1}{2} \rho V^2 S C_D$$

(3)

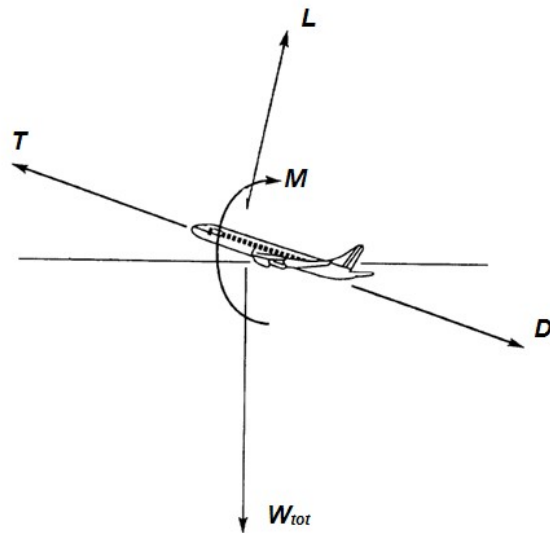


Figure 23: Basic Aerodynamic Forces [18]

Before any aerodynamic analysis is performed an understanding of the atmospheric conditions must be taken into account, to better understand what the SPACOM may encounter. The performance of an aircraft is directly related to altitude in which it is flown. Table 4 shows standard atmospheric values at sea level, 40,000 ft, and 65,000 ft.

Table 4: Atmospheric Properties [17]

Altitude	Sea Level	40,000 ft	65,000 ft
Density (sl/ft³)	0.00238	0.00059	0.00017
Pressure (lb/ft²)	2,116.20	393.1	118.9
Temperature (F°)	60	-70	-70

Figure 24, shows a how the air temperature varies with altitude.

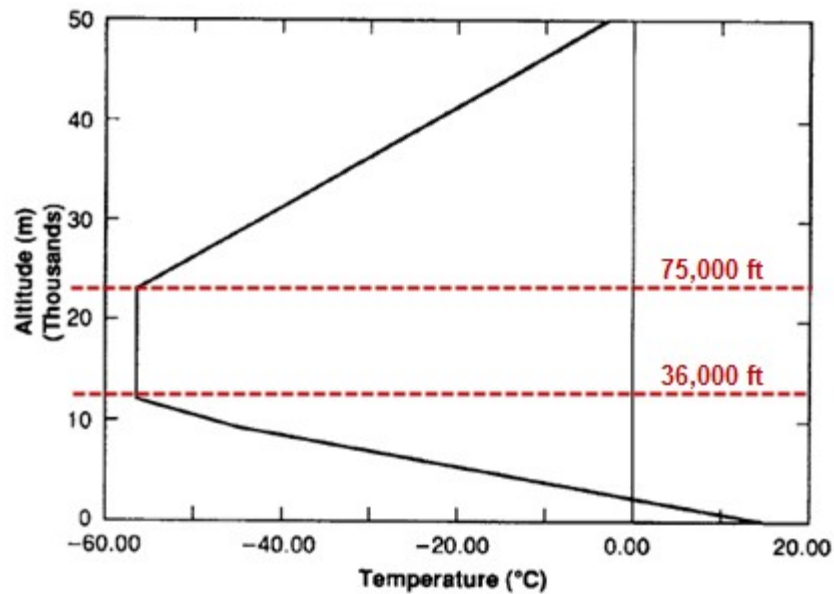


Figure 24: Air Temperature vs. Altitude [19]

As shown in figure 24, between 36,000 feet – 75,000 feet (11 km – 23 km) the air temperature is fairly constant at approximately -70°F (-57°C).

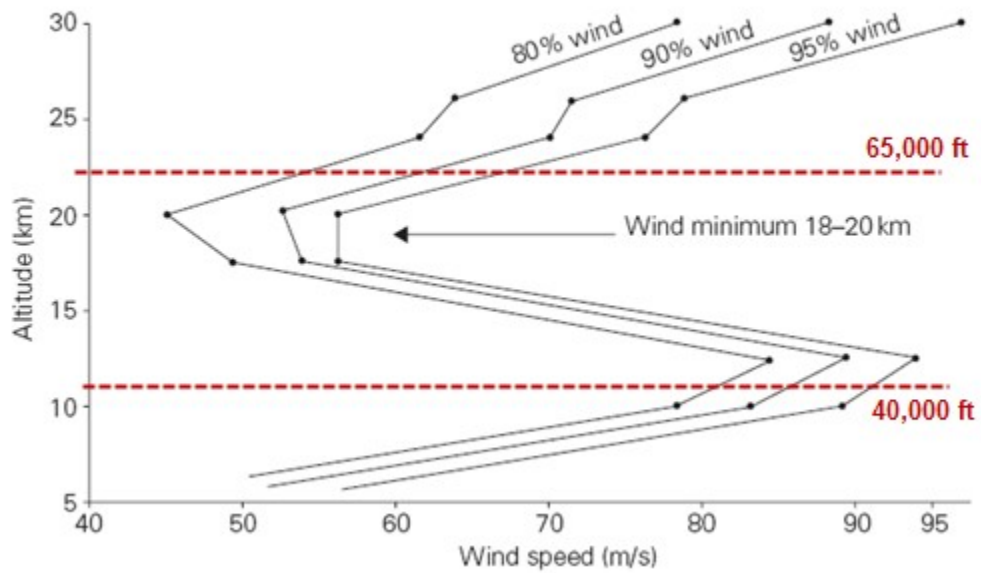


Figure 25: Wind Speed vs. Altitude [20]

Figure 25, shows the wind speeds as a function of altitude. At the maximum and minimum altitude the SPACOM will encounter the following wind speeds, Table 5.

Table 5: Wind Speed at Max. & Min. Altitudes

80%	40,000 ft	260 ft/s
	65,000 ft	175 ft/s
90%	40,000 ft	280 ft/s
	65,000 ft	200 ft/s
95%	40,000 ft	295 ft/s
	65,000 ft	215 ft/s

7.0 Preliminary Sizing

7.1 Main Wing

Since solar powered UAVs produce less thrust outputs, when compared to conventional single engine aircrafts, it is difficult to calculate the overall size of the wing. The overall wing area will depend on how many solar cells can be mounted, which will then be dependent on how much solar energy is collected.

To ensure there is enough room to mount the solar cells, a large wing area, with a high aspect ratio will be required. A high aspect ratio will result in lower induced drag, and a higher lift-to-drag ratio. A high aspect ratio will also require a large wing span as show in equation 4.

$$AR = \frac{b^2}{S}$$

(4)

Recent research has shown that a thickness ratio between 12% – 14% will result in a lower wing weight, and a higher lift value [30].

According to Raymer [2], it is ideal to have a taper when dealing with rectangular wings; an ideal taper ratio would be 0.45, this will produce a very close elliptical lift distribution. A taper ratio of 0.30 was chosen for the SPACOM, which is similar to the HELIPLAT Solar UAV design [22].

The main wing of the SPACOM will need to produce the maximum amount of lift as possible in order to achieve the mission requirements. For this reason it will incorporate a cantilevered mid-wing without any sweep. This will result in a high lift slope, and will minimize the wing weight (respectively). A *washout* twist of -5° will shall be implemented at the wing tips to enhance the tip stall. Since the SPACOM will have a large wingspan, it may encounter a natural dihedral, for this purpose a dihedral angle will not be implemented.

Assuming that the power required to maintain flight is 30 kW (which is feasible for a SPUAV), and power collected directly from the solar cells is approximately 37 W/ft². It is then calculated that approximately 810 ft² of solar cells would be required to power the aircraft; for conservative reasons the total wing area (S_w) shall be rounded to 830 ft². Assuming an aspect ratio of 30, the wing span (b_w) can be calculated using equation 5.

$$b_w = \sqrt{(AR)(S_w)} = \sqrt{(30)(830)} \approx 160 \text{ ft}$$

(5)

Since aerodynamic performance is vital to the success of the mission requirements, the SPACOM shall be considered to have characteristics of a sailplane. A sailplane is defined as glider type aircraft, which creates low amounts of drag for a given amount of lift; which is best achieved with the use of long, thin type wings.

Table 6: Wing Geometry Results

Airfoil	FX74-CL5-140
Root Chord Length	8.00 ft
Tip Chord Length	2.40 ft
Wingspan	160.0 ft
Wing Area	830 ft ²
Aspect Ratio	30.0
Taper Ratio	0.30
Wing Location	Mid-Wing
Thickness Ratio	14%
Sweep Angle	0°
Twist Angle	-5.0°
Dihedral Angle	0°

7.2 Empennage

The empennage configuration shall be two horizontal stabilizers and two rudders on each side of the tail. This will help distribute the load over the empennage, as opposed to a *T-Tail* configuration.

Since the horizontal tail may also be used mount solar cells, the initial span of the tail shall be oversized to allow as much solar cells as possible. For this matter the wing-to-tail

ratio $\frac{S_t}{S_w}$, shall be assumed to be approximately 0.40. This will allow for the spars which connect the empennage to the main wing to be connected at the mid-span of the wing.

The horizontal tail volume coefficient is defined as,

$$V_h = \frac{X_h S_h}{S_w c}$$

(6)

$$V_v = \frac{X_v S_v}{S_w b}$$

(7)

Where X_h and X_v are defined as the distance from the mean aerodynamic chord of the horizontal and vertical stabilizer's to the center of gravity of the aircraft.

Since the empennage is a twin-boom, the horizontal and vertical control surfaces will have the same chord. The empennage will be connected to the main wing with two spars, for uniformity the spars will be near the half span of each wing (~30 ft). This will decrease the stress and strain during natural dihedral stress on the main wing during flight.

Table 7: Empennage Geometry Results

Parameter	Horizontal	Vertical (2X)
Type	Twin-Boom	
Chord	5.0 ft	5.0 ft
Span / Height	20.0 ft	6.0 ft
Area	100 ft ²	30 ft ²
Aspect Ratio	4.0	1.2
Sweep Angle	0°	N/A
Thickness Ratio	12%	12%
Dihedral Angle	0°	N/A
Twist Angle	0°	N/A
Taper Ratio	0	N/A

According to Roskam [30] V_h ranges from 0.20 – 0.60 for conventional aircrafts; assuming the following values as show in Table 8 yields a V_h of 0.30. This is assuming the mean aerodynamic chord of the horizontal stabilizer is approximately 30% of the chord.

Table 8: Horizontal Tail Volume Coefficient Variables

X_h	20 ft
S_h	100 ft ²
S_w	830 ft ²
c_w	8.0 ft

Furthermore, according to Roskam [30] V_v is ranges from 0.01 – 0.05 for conventional aircrafts; assuming the following values as show in Table 9 yields a V_v of 0.012.

Table 9: Vertical Tail Volume Coefficient Variables

X_v	25 ft
S_v	60 ft ²
S_w	830 ft ²
b	160 ft

7.4 Configuration Selection

Prior to determining the overall configuration of the SPACOM, an analysis on different types of configurations was performed. The first type of configuration is the flying wing configuration as shown in Figure 26, which is similar to Helios.



Figure 26: Flying Wing Configuration

This type of configuration is good if the weight is evenly distributed over the span of the wing, however referring back to the Helios crash incident it would seem the SPACOM may encounter the same excessive dihedral problems.

The second type of configuration is the conventional configuration, as shown in Figure 27; this type of configuration is mostly commonly used today. This configuration may not be the best choice for the SPACOM due to the majority of weight being distributed in the center of the aircraft.

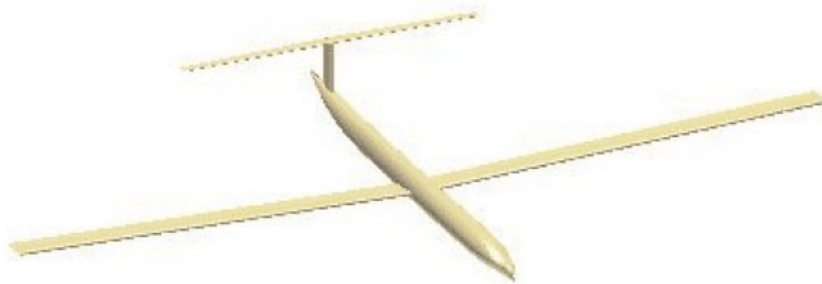


Figure 27: Conventional Configuration

The third type of configuration is the twin boom configuration, as shown in Figure 28; this type may be the best fit for the SPACOM. The twin boom not only doubles the amount of surface area than the flying wing but also increases the structural ability as well.

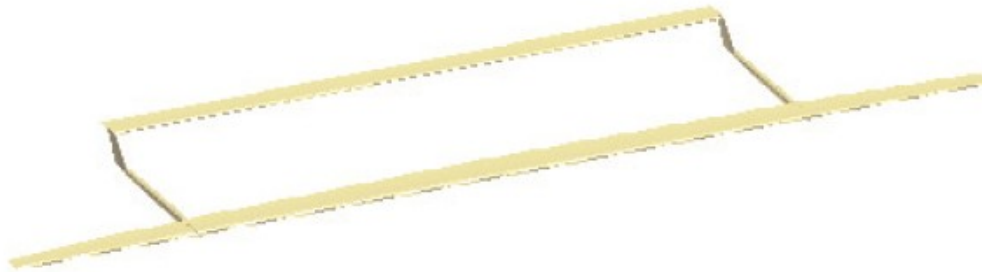


Figure 28: Twin Boom Configuration

7.5 Fuselage

The fuselage shall be used store mission critical sub-systems, such as:

- Auto-pilot
- GPS
- Communication systems
- Camera(s)
- Fuel cell(s)

The fuselage must be designed as to not affect the performance of the wing or empennage, but needs to be robust enough to support the listed sub-systems. For this purpose, the fuselage is chosen to mimic the shape of an *airfoil*.

By giving the fuselage the *airfoil* configuration it allows the more surface area for any extra solar cells (if needed). It also will blend the body of the wing, which may decrease any induced drag.

7.6 Drive train

To achieve higher thrust without sacrificing high amounts of energy, electric motors shall be used to power the SPACOM. Electric motors are generally expressed in units of horsepower (*hp*), which is defined as:

$$hp = \frac{T_0 \omega}{6,600}$$

(8)

Where T_0 is the required torque and ω is the angular velocity. For efficiency purposes, brushless DC electric (BLDC) motors were chosen for the SPACOM. Brushless DC motors use permanent magnets which are used to rotate a fixed rotor and/or arm; this increases reliability, efficiency, power, and reduces noise. The characteristics of a standard BLDC with respect to the speed and torque can be found as shown in Figure 36.

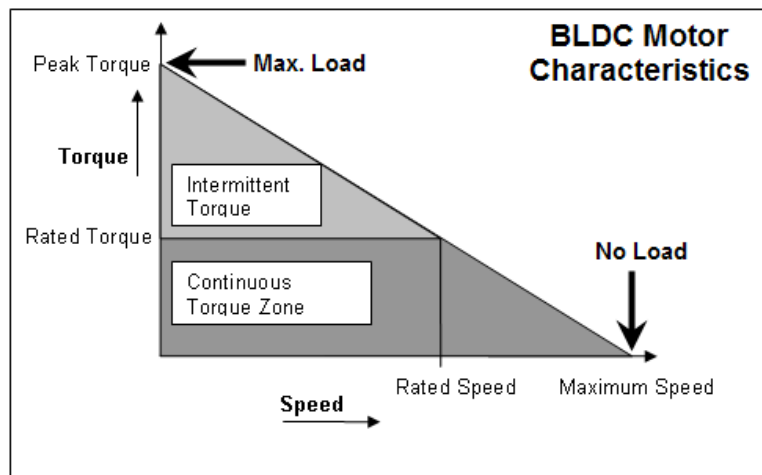


Figure 29: BLDC Motor Speed vs Torque Characteristics [12]

It has been found that using rare earth magnets such as Samarium Cobalt (Sm-Co) reduces the amount of electromagnetic interference which is present in conventional electric motors [23]. Sm-Co BLDC motors are have been implemented on the Space Shuttle elevons. The motor produces approximately 12.9 kW (17.1 hp) at 9,000 rev/min and weighs approximately 10 lbs. In recent tests Sm-Co BLDC motors have recorded an operating efficiency of 95%; this is due to its high magnetic density [23]. The BLDC motors shall be conjoined with an appropriate speed reduction control system in order to drive relatively large, slow turning propellers.

7.7 Airfoil Selection

7.7.1 Wing Airfoil

In determining an optimal wing configuration for the SPACOM, various airfoils were analyzed to determine which would be most beneficial. The three airfoils which were considered were: Selig S1223, Liebeck LA2573A, and the Wortmann FX 74-CL5-140; characteristics of these airfoils are as described.

S1223

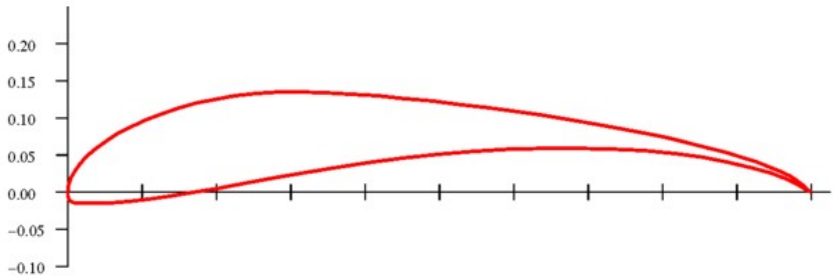


Figure 30: Selig S1223 Size Characteristics [13]

LA2573A

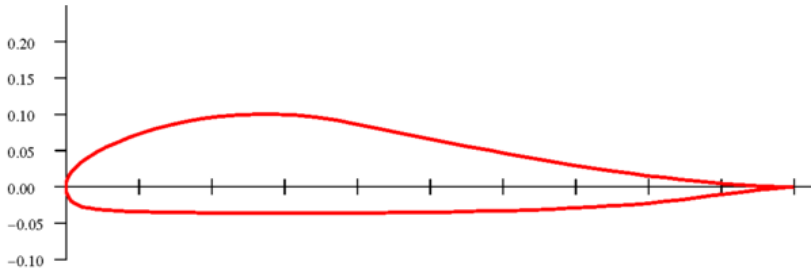


Figure 31: Liebeck LA2573A Size Characteristics [13]

FX 74-CI5-140

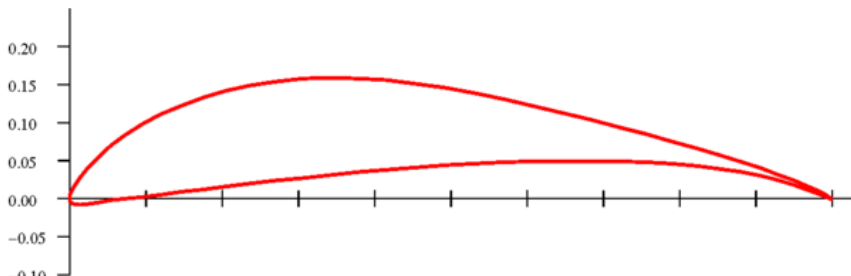


Figure 32: Wortmann FX 74-CL5-140 Size Characteristics [13]

The aerodynamic characteristics of the following airfoils are shown in Table 10 below:

Table 10: Airfoil Aerodynamic Comparison [13]

Airfoil	S1223	LA2573A	FX 74-CL5-140
Thickness (%)	12.1	13.7	13.1
Camber (%)	8.7	3.2	9.7
Trailing Edge Angle (°)	12.1	7.0	5.3
Lower Flatness (%)	17.6	56.1	27.6
Leading Edge Radius (%)	3.1	3.2	1.8
Max C_L	2.425	1.183	2.275
Max C_L Angle (°)	8.0	15.0	9.0
Max L/D	71.86	18.556	73.594
Max L/D Angle (°)	5.5	10.5	0.5
Stall Angle (°)	8.0	1.0	3.5
Zero-Lift Angle (°)	-13.5	-3.0	-11.5

All three airfoils as described above all share beneficiary traits which can be used for the SPACOM. The airfoils were analyzed using XFLR5 v6.0, which is a program similar to X-Foil. The airfoils were analyzed from various Reynolds number ranges ($1.0 \times 10^5 - 4.0 \times 10^6$, with 1.0×10^5 intervals) and angles of attack (-10° to 15°).

The Reynolds number is defined as:

$$Re = \frac{\rho V x}{\mu}$$

(9)

The Reynolds number for the FX 74-CL5-140 airfoil at the required mission altitudes is calculated to be the following:

Table 11: Reynolds Number over Wing with Respect to Altitude

Altitude (ft)	Reynolds Number (c_o)	Reynolds Number (c_t)
Sea Level	1.30×10^6	0.40×10^6
40,000	0.80×10^6	0.25×10^6
65,000	0.50×10^6	0.15×10^6

Main Wing Reynolds Number

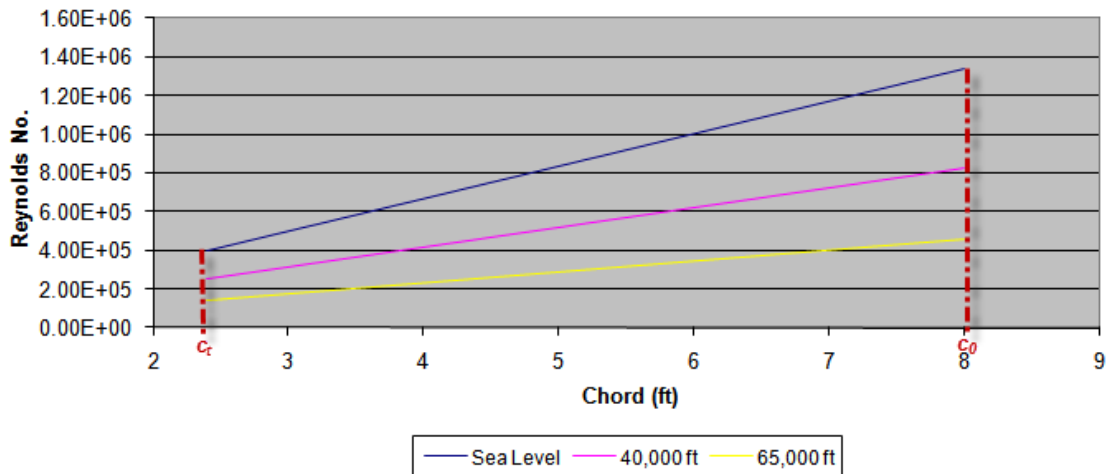


Figure 33: Reynolds Number over Chord of Wing

Using the data from XFLR5 it was found that a significantly higher C_l was achieved with increasing angle of attack for FX 74-CL5-140 airfoil. The solutions for C_l vs C_d , C_l vs AoA , C_m vs AoA , and C_l/C_d vs AoA (FX 74-CL5-140 only) are shown below. In retrospect, all three airfoils would make good candidates for the SPACOM, but FX 74-CL5-140 was chosen for the main wing; not taken into consideration was the validity of the XFLR5 program.

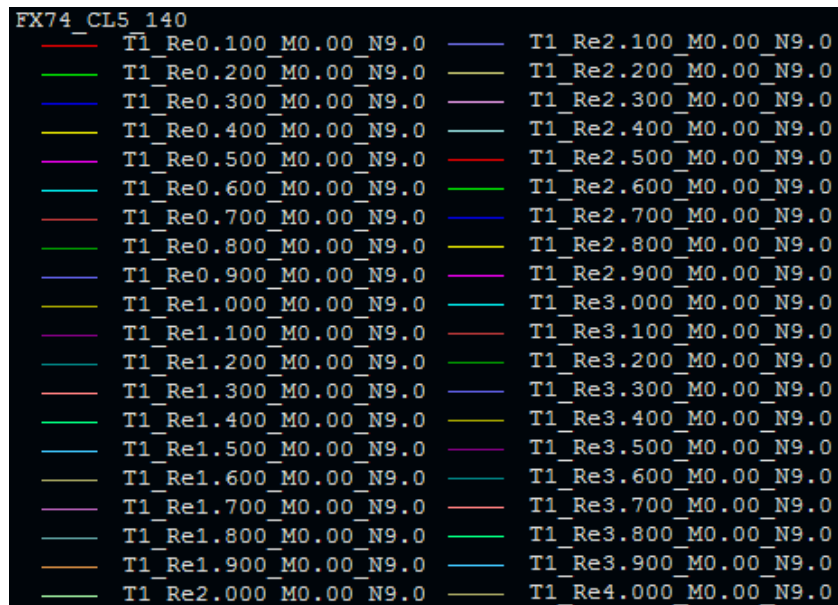


Figure 34: Reynolds Number Range Legend

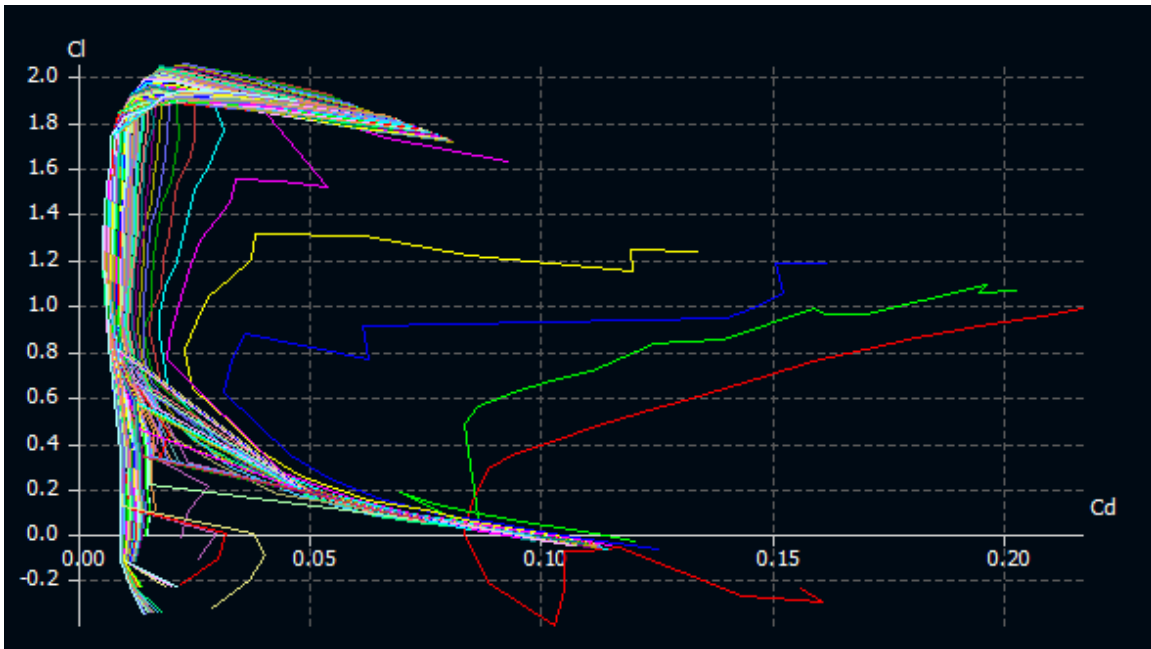


Figure 35: FX 74-CL5-140 C_l vs C_d

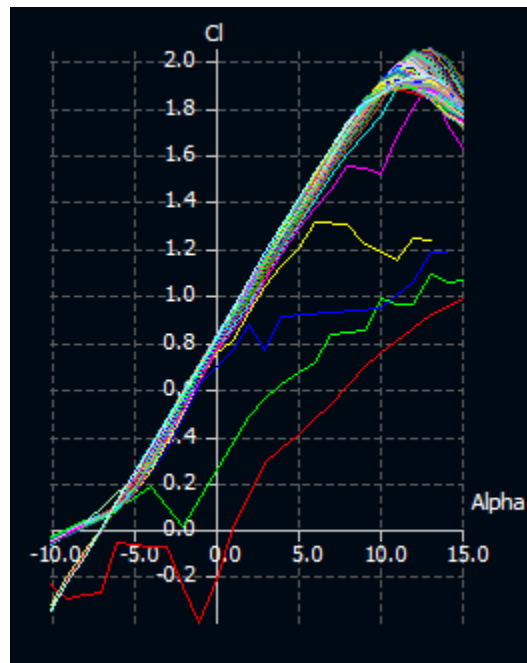


Figure 36: FX 74-CL5-140 C_l vs AoA

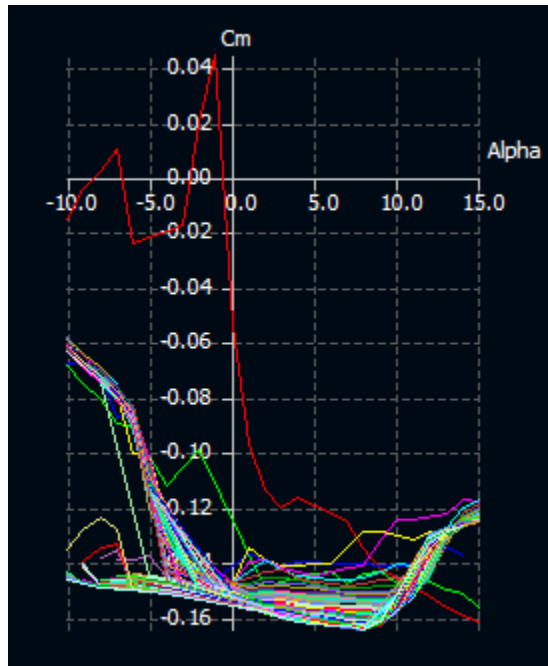


Figure 37: FX 74-CL5-140 C_m vs AoA

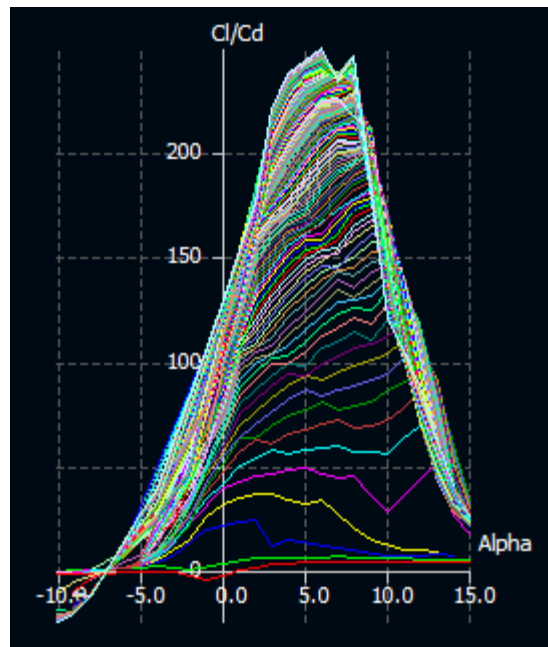


Figure 38: FX 74-CL5-140 C_l/C_d vs AoA

7.7.2 Empennage Airfoil

The empennage shall serve as the primary horizontal and vertical stabilizers, for this reason the NACA 0008 airfoil was chosen. Due to its low thickness, the airfoil shall result in lower induced drag, and will be respectively lighter in overall weight. The sizing characteristics of the airfoil are shown below.

NACA 0008

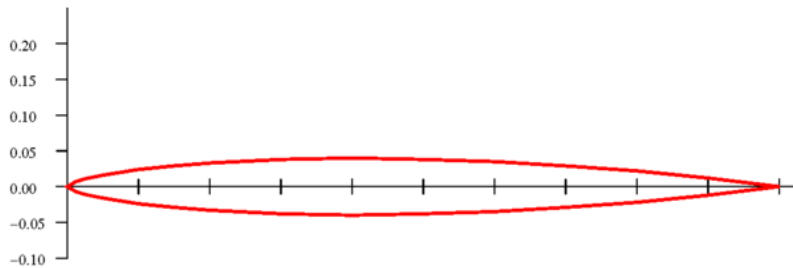


Figure 39: NACA 0008 Size Characteristics [13]

Table 12: NACA 0008 Characteristics [13]

Airfoil	NACA 0008
Thickness (%)	8.0
Camber (%)	0
Trailing Edge Angle (°)	14.2
Lower Flatness (%)	74.5
Leading Edge Radius (%)	2.2
Max C_L	0.586
Max C_L Angle (°)	11.0
Max L/D	23.164
Max L/D Angle (°)	3.0
Stall Angle (°)	3.0
Zero-Lift Angle (°)	-3.0

Again an aerodynamic analysis on the airfoil was conducted using XFLR5, with a Reynolds number range of $(5.0 \times 10^4 - 1.0 \times 10^6)$ and an AoA range of -5 to +5, results are shown in the following figures.

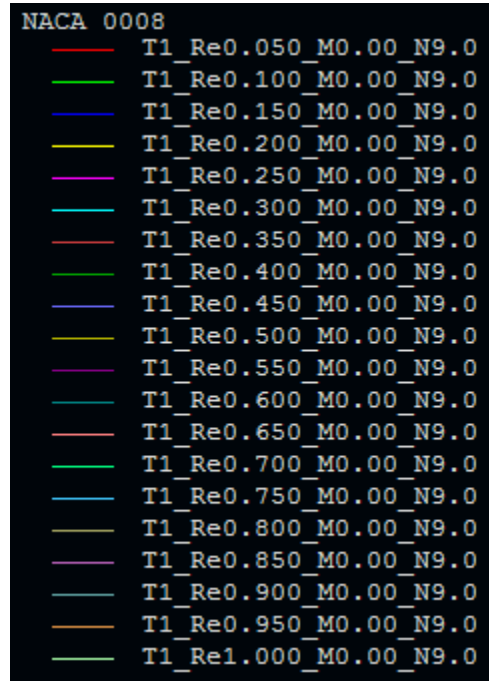


Figure 40: Reynolds Number Range Legend

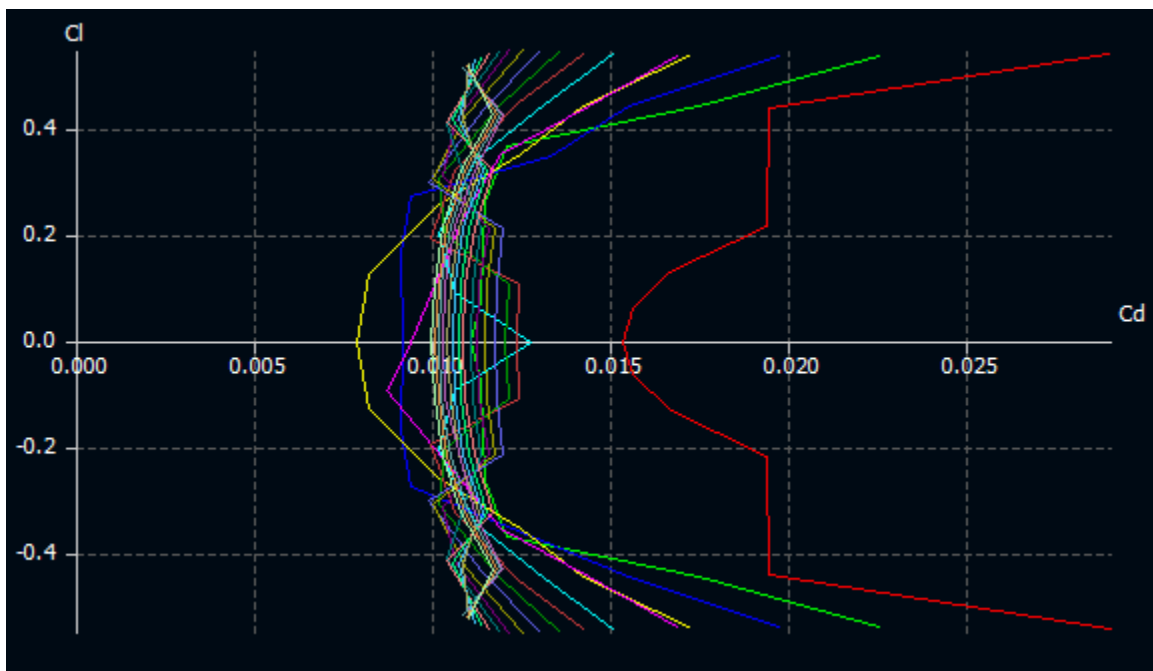


Figure 41: NACA 0008 C_l vs C_d

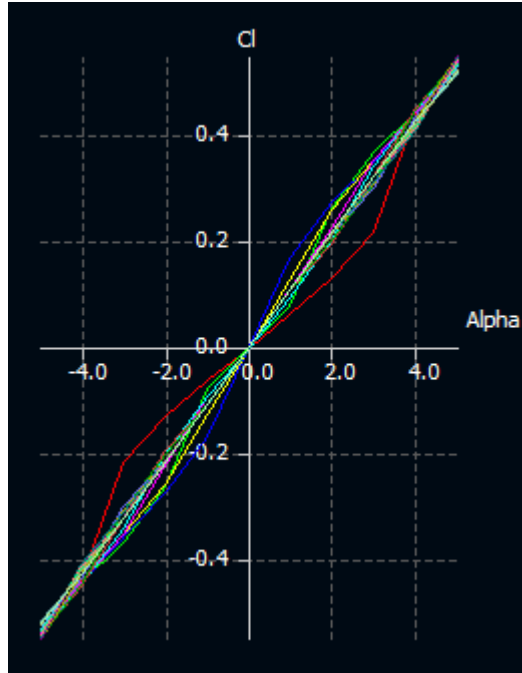


Figure 42: NACA 0008 C_l vs AoA

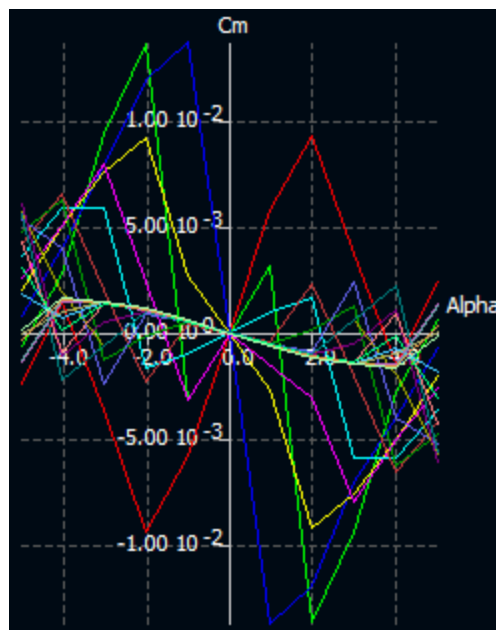


Figure 43: NACA 0008 C_m vs AoA

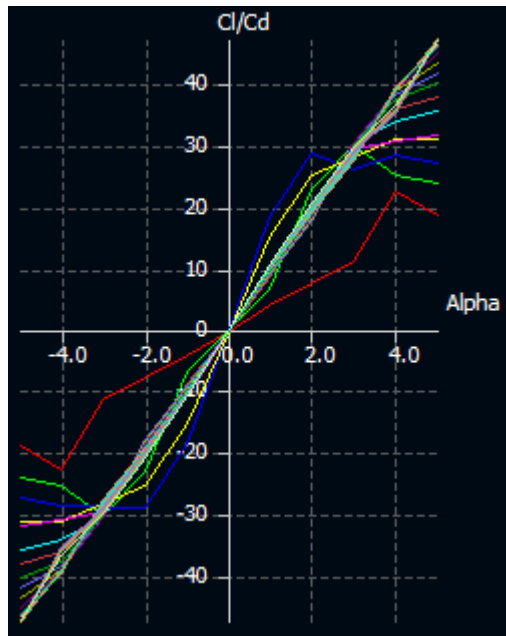


Figure 44: NACA 0008 C_l/C_d vs α

8.0 Control Surface

8.1 Horizontal Stabilizer

Historical trends have shown a 0.28 – 0.34 ratios for aileron chord to wing chord [15]. Historical trends have also shown a 0.40 – 0.50 ratios for elevator to horizontal chord [30]. In order to have the maximum surface area onto the wing surface to be used for solar cells, no ailerons shall be implemented on the control surfaces.

The elevator will be located on the horizontal control surface; we will assume a ratio of 0.50 due to the size of the SPACOM. One elevator shall be placed on the empennage as shown in Figure 45.

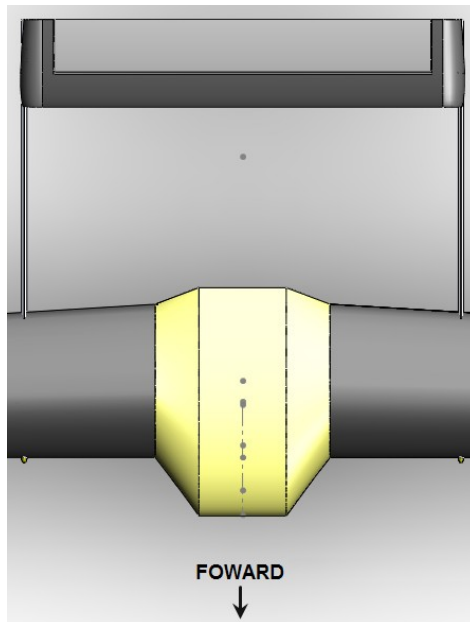


Figure 45: Horizontal stabilizer Sizing

Table 13: Elevator Sizing

Airfoil	NACA 0008
Span	17.0 ft
Chord	2.5 ft

8.2 Vertical Stabilizer

The implementation of two vertical stabilizers will allow a larger surface area without having to increase the size of the empennage. It will also allow for higher rudder authority during flight at respectively low speeds. Historical trends have shown a 0.35 – 0.40 ratios for rudder to vertical chord. Due the size of the SPACOM, a ratio of 0.40 shall be used for the sizing.

Since there are no ailerons on the main wing of the SPACOM, the rudders must supply sufficient yawing capabilities. Since the SPACOM will encounter a natural dihedral during flight, it will allow the SPACOM to roll with the combination of yawing.

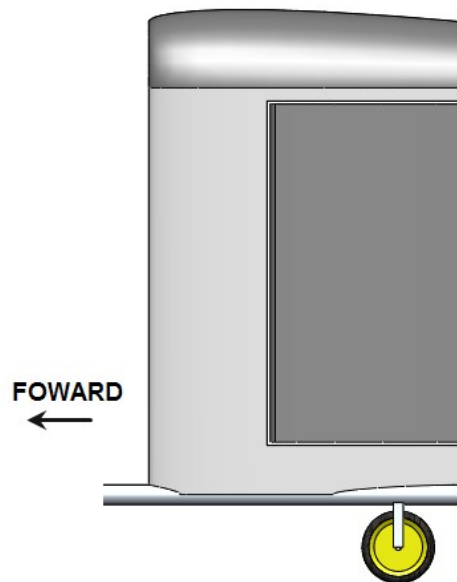


Figure 46: Vertical Stabilizer Sizing

Table 14: Rudder Sizing

Airfoil	NACA 0008
Height	4.0 ft
Chord	2.0 ft

9.0 Landing Gear

Due to the large size of the SPACOM, the landing gear must suffice to disallow any damage to the structure when it's on the ground. For this reason, the SPACOM shall employ six points of ground contact. Four lightweight gears shall be placed in line with each other along the horizontal axis of the main wing. Furthermore, two wheels shall be placed at the end of the structure bars connecting the empennage to the fuselage.

Due to the massive wingspan, two break away gears shall protect the drooping wing tips from hitting the ground. These break away gears, are not physically connected to the main wing. The difference between the height of the front and aft of the aircraft shall be a difference of approximately 20 inches (1.70 ft); on a level runway the nose of the SPACOM will be approximately 6° higher. This will allow for more clearance of the propellers.

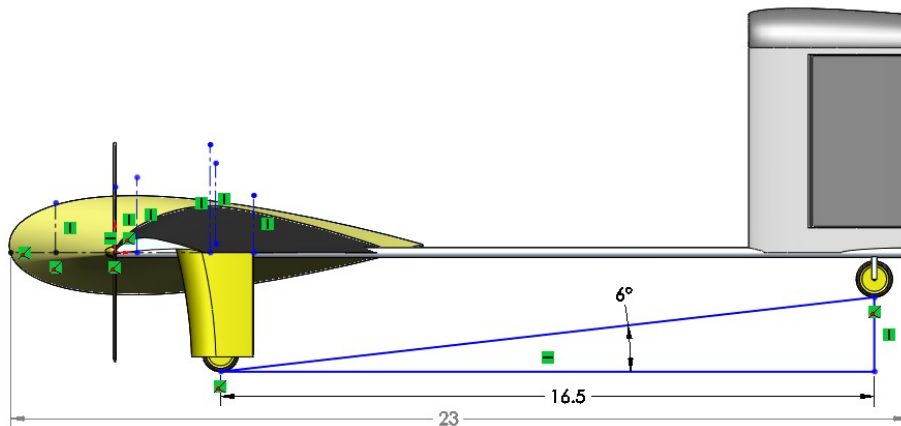


Figure 47: Landing Gear

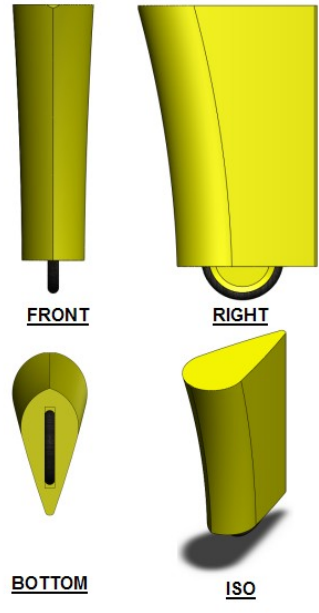


Figure 48: Main Landing Gear Layout

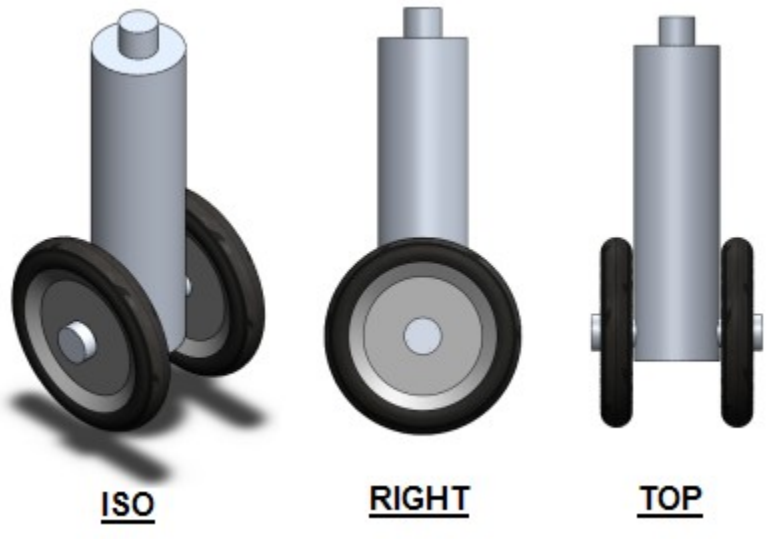


Figure 49: Breakaway Landing Gear Layout

10.0 Weight Analysis

10.1 Airframe Weight

The aircraft when empty is defined as not including a payload(s), mission critical instruments, solar cells, fuel cells, and the drive train. The total weight of the airframe (W_{af}) can be estimated using the following equation for calculating the airframe weight of a sailplane [31].

$$W_{af} = A(S_w b^3)^B$$

(10)

Where A and B are ultimate load coefficients; in recent studies it has been found that for ultra-light, cantilever wings, with twin-boom tail sailplanes, $A = 0.311$ and $B = 0.310$

[31]. Using these values the total weight of the airframe is found to be 280 lbs, for the case of this study the weight of the air frame shall be rounded up to 300 lbs to include the empennage.

10.2 Solar Cells

As previously noted, the power required for the SPACOM is assumed to be 30 kW. It is essential to equip the SPACOM with the lightest, most efficient solar cell available. A single *Spectrolabs* solar cell weighs approximately 0.172 lbs/ft² [24]. Assuming the total top surface area of the aircraft will be covered in solar cells, the total weight of the solar cells is approximately 195 lbs. This overall weight can be distributed equally over the main wing.

10.3 Fuel Cell

As specified in the previous section, $H_2 - O_2$ fuel cells shall be used as the primary source of power during night time flight of the SPACOM. In order to accommodate the power requirements, three fuel cells shall be used, totaling to approximately 450 lbs. The fuel cells are vital to the SPACOM, thus they shall contain the most percentage of weight.

10.4 Payload

The payload is defined as components and/or instruments that are required in order for the mission requirements to be successful. For this study the weights of these sub-systems shall be assumed to be a total of 100 lbs.

10.5 Gross Weight & Balance

The total weight of the SPACOM can now be estimated as shown in the Table 15 below.

Table 15: Weight Estimate Breakdown

Sub-System	Weight (lbs)
Wing	270
Empennage	20
Fuel Cell (3X)	450
Solar Cells	195
Propellers (4X)	35
Fuselage	10
Forward Landing Gear (4X)	40
Rear Landing Gear (2X)	10
Support Bar (2X)	10
Payload	100
Total	1,140

The airframe weight loading is then approximated to be 1.25 lbs/ft², which is feasible considering the weight loading for most aircraft ranges between 1.0 lbs/ft² and 2.0 lbs/ft².

Now that all the weight estimates have been made, they can now be placed on a horizontal axis as shown in Figure 50 below. The aerodynamic center is placed approximately 25% of the chord of the wing; which is approximately 2.0 ft from the *LE* of the wing (4.5 ft from the nose). Dividing the sum of the moment arms by the total weight, the *CG* is approximately 1.3 ft from the *LE* of the wing (3.8 ft from the nose); this distance is approximately 0.7 ft forward of the aerodynamic center.

Figure 50, shows the center of gravity of all the major components and their distances with respect to the center of gravity of the aircraft.

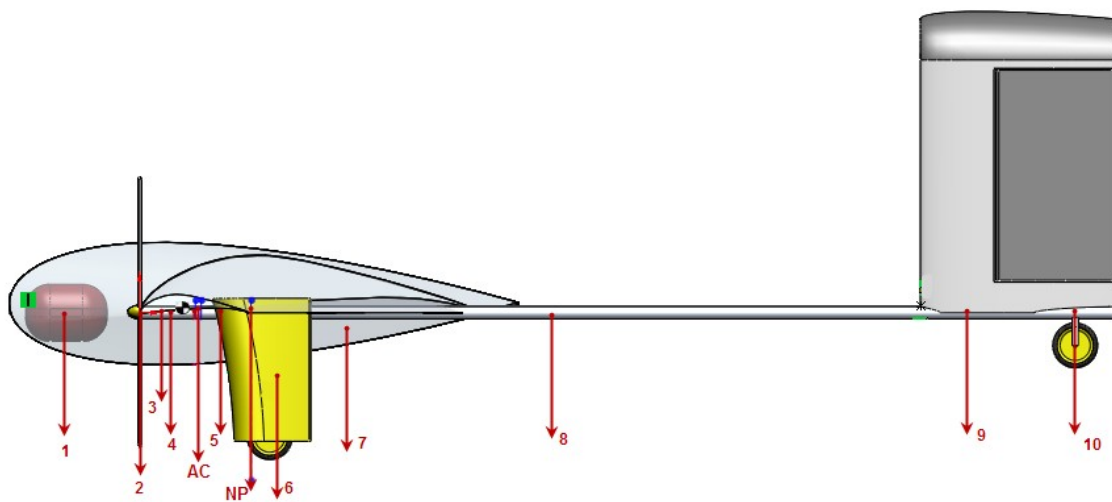


Figure 50: SPACOM Weight & Balance

Table 16: Sub-System Distance Moment

No.	Sub-System	Distance From Nose (ft)	Moment Arm (ft·lbs)
	Center of Gravity	3.8	
AC	Aerodynamic Center	4.5	
NP	Neutral Point	4.9	
1	Fuel Cell (3X)	1.0	450
2	Propellers (4X)	2.5	88.0
3	Fuselage	3.5	35.0
4	Wing	5.5	1485
5	Solar Cells	5.5	1,073
6	Forward Landing Gear (4X)	5.7	228
7	Payload	7.0	700
8	Support Bar (2X)	15.0	150
9	Empennage	19.0	380
10	Rear Landing Gear (2X)	22.0	220
		Total	4,808

11.0 Stability & Controls

11.1 Static Longitudinal Stability

Static longitudinal stability is defined as ability of an aircraft to return to equilibrium after an unexpected change in direction in the lateral direction is caused (by an upward gust).

This is critical for the SPACOM due to the high wind speeds at extreme altitudes; the SPACOM must be longitudinally stable to keep it from losing control.

The mean aerodynamic chord can be found using,

$$\bar{X}_{ac} = \frac{\left[\bar{X}_{acw} + \left\{ C_{L\alpha_h} \left(1 - \frac{\partial \epsilon}{\partial \alpha} \left(\frac{S_h}{S} \right) \bar{X}_{ac_h} \right) \right\} \right]}{\left[1 + \left(C_{L\alpha_h} \left(1 - \frac{\partial \epsilon}{\partial \alpha} \left(\frac{S_h}{S} \right) \right) \right) \right]}$$

(11)

Using the values from the Weight & Balance section, and the data collected from the XFLR 5 program, the results in Table 17 can be determined.

Table 17: Mean Aerodynamic Chord Properties

\bar{X}_{acw}	0.25 ft
$C_{L\alpha_h}$	0.1 ft
$\frac{\partial \epsilon}{\partial \alpha}$	0.286
S_h	100 ft ²
S	830 ft ²
\bar{X}_{ac_h}	11.75 ft

Figure 51 shows the results on the longitudinal X-Play using various values of S_h ,

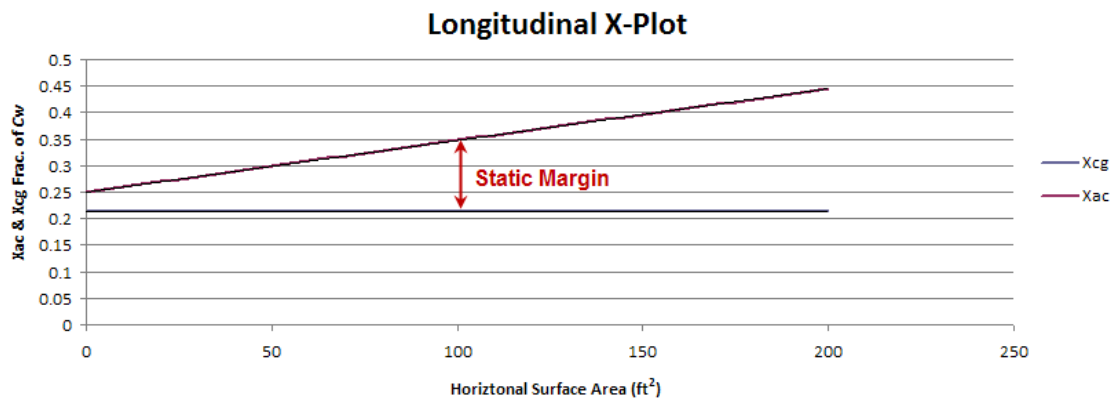


Figure 51: Longitudinal X-Plot

Since the SPACOM will not use any fuel which will affect the overall weight, the location of the CG will not move, thus being constant. Using the current empennage design sizing ($S_h = 100$ ft^2), the static margin is approximately 20%. Considering that the static margin of a conventional aircraft is between 5% – 15%.

Low static margin allows for less static stability which requires higher elevator authority. High static margin results in relatively higher static stability, but reduces the required elevator authority.

11.2 Static Directional Stability

The directional stability X-Plot is shown in Figure 52.

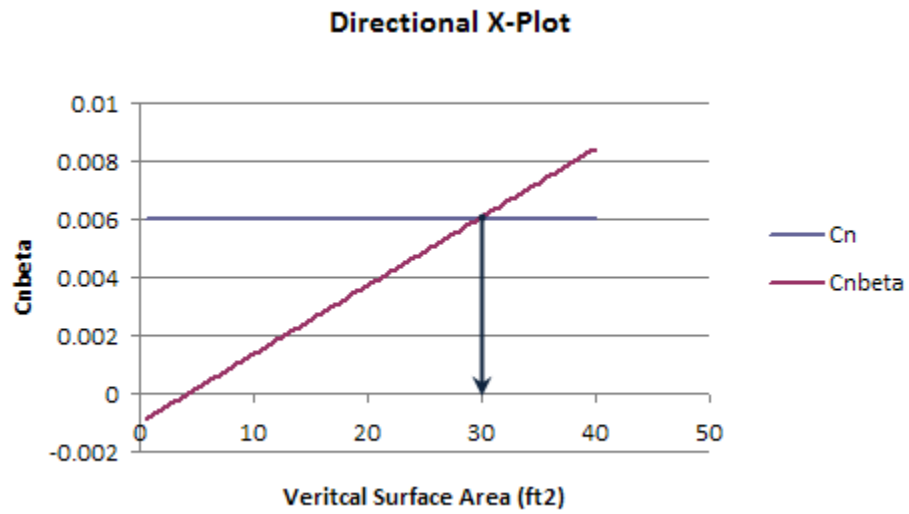


Figure 52: Directional X-Plot

12.0 Performance

12.1 Power Performance

For the purpose of this study, the SPACOM shall soar through the skies of Iraq, which is located 33° N latitude; during the month of June, when the sunlight duration is at the maximum. Figure 53, illustrations how the power from the solar cells and the fuel cells will be distributed throughout the day. As shown, the solar cells will not generate enough energy to power the SPACOM until approximately 7:00 am, and will continue to produce until approximately 5:30 pm.

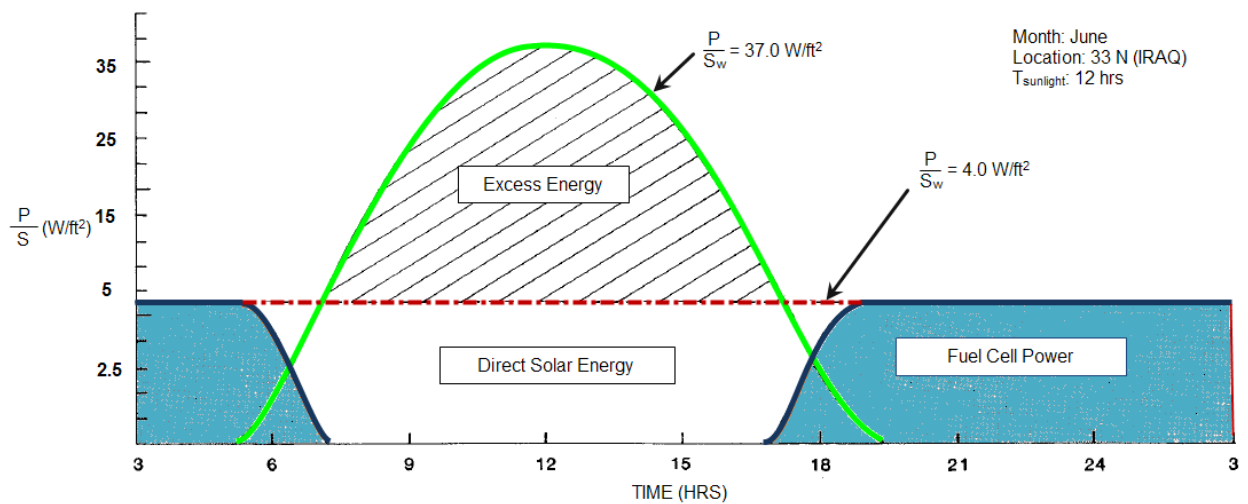


Figure 53: Power Breakdown during Flight

12.2 Take-off Performance

The power required for the SPUAV to maintain altitude at steady and level flight, is defined as the thrust required is equal to the total drag and the aircraft's weight divided by the lift-to-drag ratio.

The thrust requirement for the SPACOM during initial takeoff and during climbing conditions is expressed by,

$$T = D + W \sin \gamma$$

(12)

Where γ is the climb angle of the aircraft; assuming a rotation and climb angle of 5 degrees where C_L is approximately 1.5, the maximum total thrust required is $D + 90$ lbs. This yields a total thrust requirement of approximately 110 lbs during take-off.

The flight velocity can be expressed using,

$$V_{\infty} = \sqrt{\frac{2W}{\rho S C_L}}$$

(13)

The distance required for the SPACOM to take off can be defined as,

$$S_{LO} = \frac{1.44W^2}{g\rho S C_{L,\max} \{T - [D + \mu_r(W - L)]\}}$$

(14)

To ensure a margin of safety during takeoff, the liftoff velocity (V^{LO}) is typically 20%

higher than the stalling velocity, hence

$$V_{LO} = 1.2V_{stall} = 1.2\sqrt{\frac{2W}{\rho_{\infty} S C_{L,\max}}}$$

(15)

Using equations as described above, it would require approximately 981 feet for the SPACOM to successfully lift off. This is based off the thrust requirements, however if the SPACOM does not meet the takeoff requirements it will require a much longer distance to takeoff. For this reason the SPACOM shall have an assisted takeoff by a pulley system or a standard ground vehicle to ensure the SPACOM can achieve the required take-off thrust every time.

12.3 Flight Performance

The stall speed of the SPACOM can be found using the following equation,

$$V_{Stall} = \sqrt{\frac{2W}{\rho S C_{L_{max}}}}$$

(16)

Where $C_{L_{max}}$ is assumed to be 2.0, which is slightly below the maximum amount the wing airfoil can achieve. Knowing the weight the stall speed at various altitudes can be determined, as shown in Table 18.

Table 18: Stall Speed vs. Altitude

Altitude (ft)	Stall Speed (ft/s)	Cruise Speed (ft/s)
Sea Level	25	27
40,000	49	57

65,000	88	101
---------------	----	-----

The rate of climb can be determined using,

$$R / C = V_{\infty} \sin \alpha$$

(17)

At sea-level conditions the SPACOM will travel at a speed of approximately 26 ft/s (18 mph), assuming a climb angle of 5° it would take approximately one hour to reach 10,000 ft. The climb rate increases as the SPACOM increases in altitude due to the decreasing air density. Figure 54 below shows how quickly R/C increase with altitude.

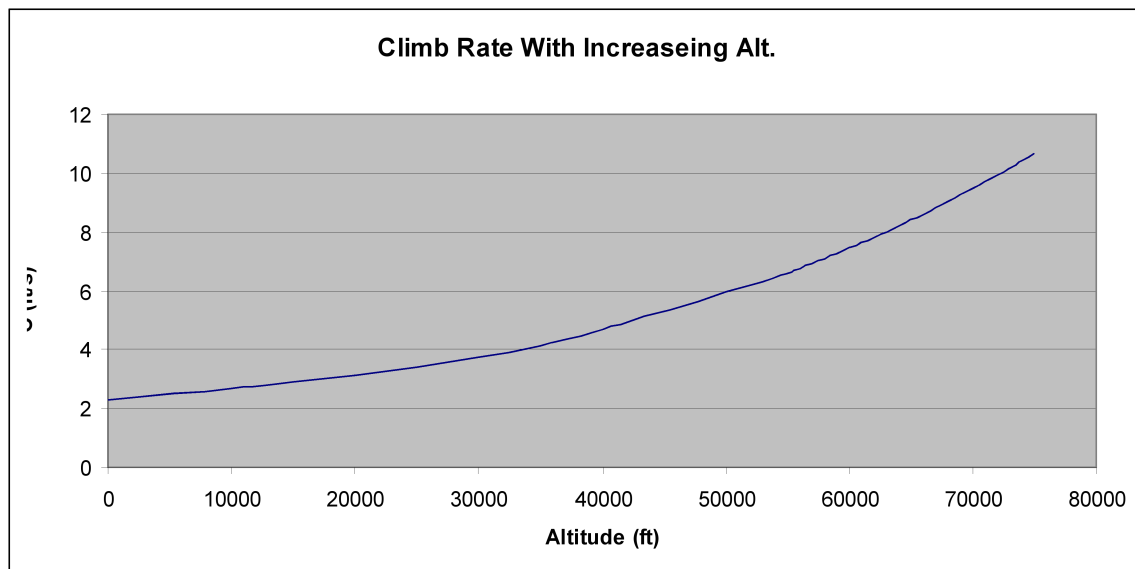


Figure 54: Climb Rate with Increasing Altitude

It should take no more than three hours for the SPACOM to reach its maximum altitude of 65,000 ft.

The power required to sustain flight can be found using,

$$P_R = T_R V_{\infty} \eta^{-1}$$

(18)

Figure 55, shows how the power required increases with altitude; this is all assuming an overall efficiency of 85%. This shows that a maximum of approximately 4.0 kW is required to keep the SPACOM in flight at 65,000 feet.

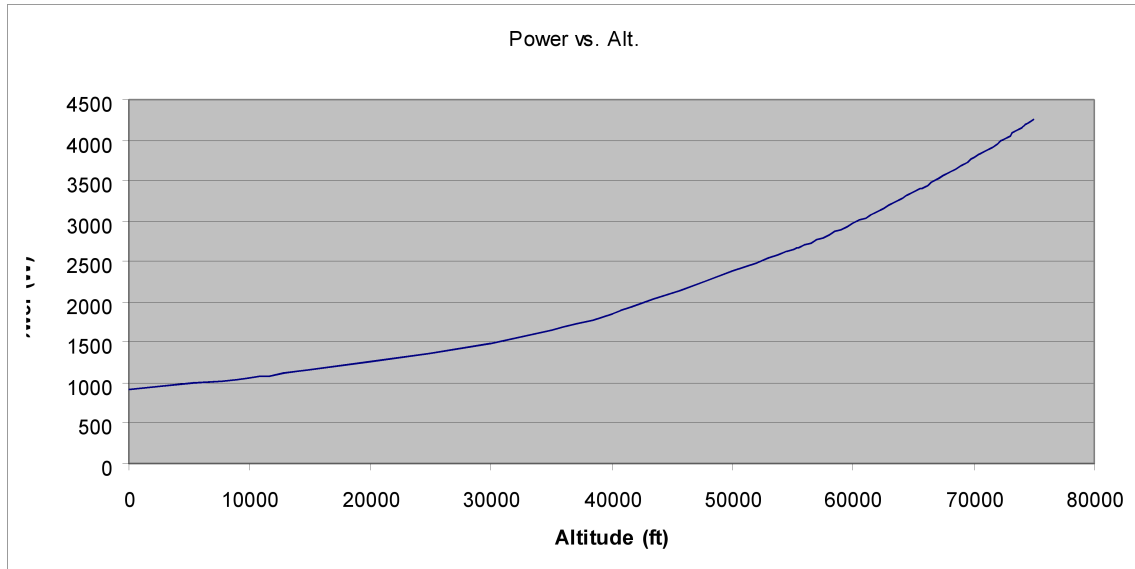


Figure 55: Power with Respect to Altitude

Respectively it would seem feasible that the power required would only increase to allow for the increasing velocity required to keep the SPACOM at the required altitude, as shown in Figure 56, Figure 57, and Figure 58.

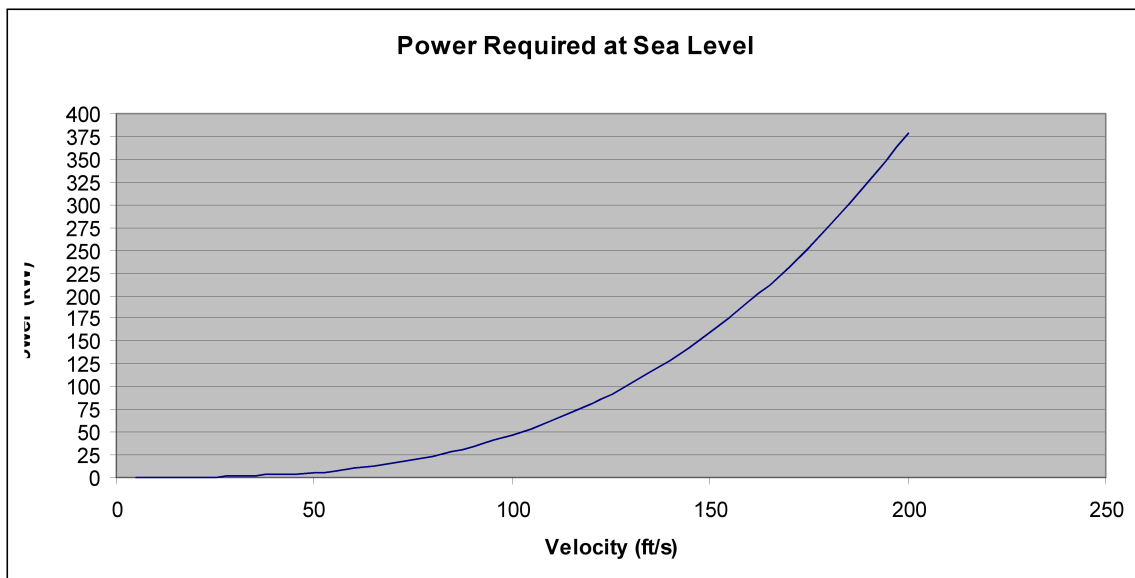


Figure 56: Power Required at Sea Level

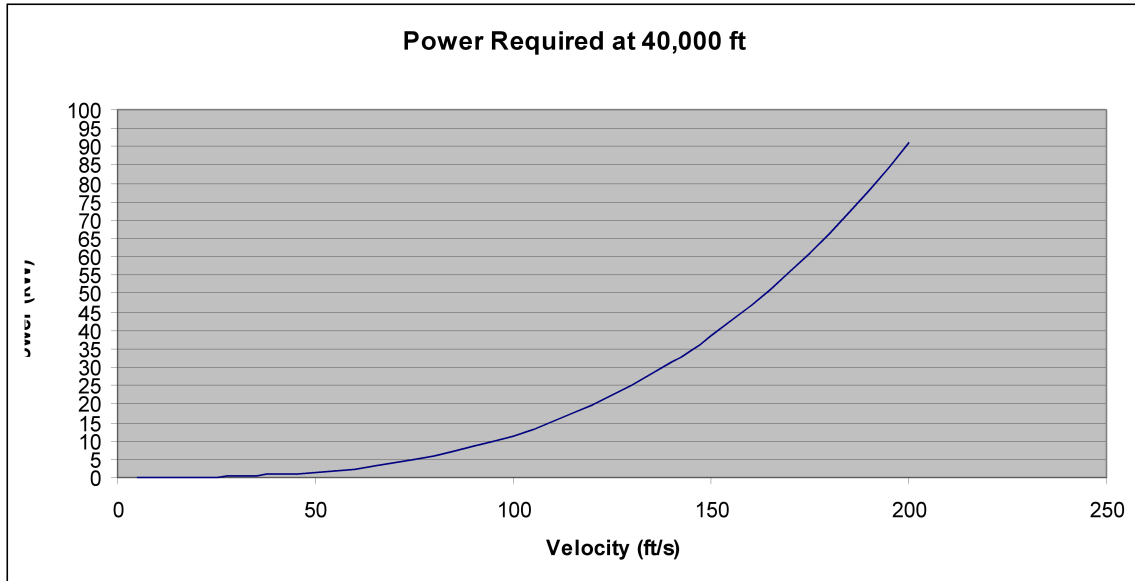


Figure 57: Power Required at 40,000 ft

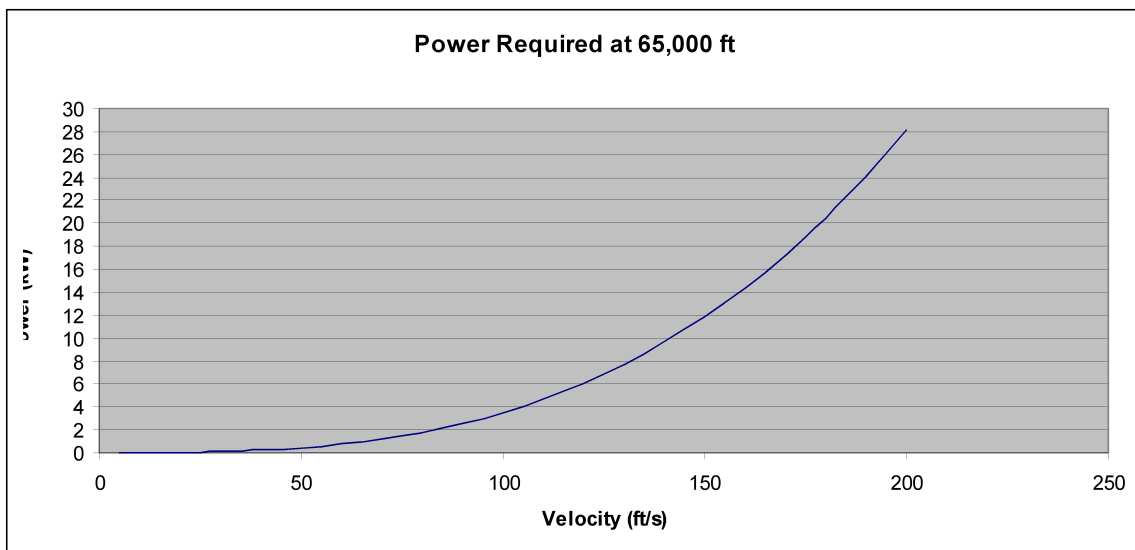


Figure 58: Power Required at 65,000 ft

Table 19: Power Requirements with Altitude

Altitude (ft)	Cruise Speed (ft/s)	Power Required
Sea Level	27	1.07 kW
40,000	57	2.18 kW
65,000	101	3.93 kW

Since there may be a significant loss in power during night flight, it is critical to measure how the altitude effects during night flight. The descent rate can be found using,

$$R / D = \frac{V_{\infty} \sin \gamma}{\left(\frac{L}{D} \right)}$$

(19)

Respectively, γ shall be assumed to -5° ; this yields a descent rate of approximately 600 ft/hr at 65,000 ft, as shown in Figure 59. This results in a total of 7,000 ft altitude loss if the SPACOM were to maintain that rate of descent during a twelve hour night period.

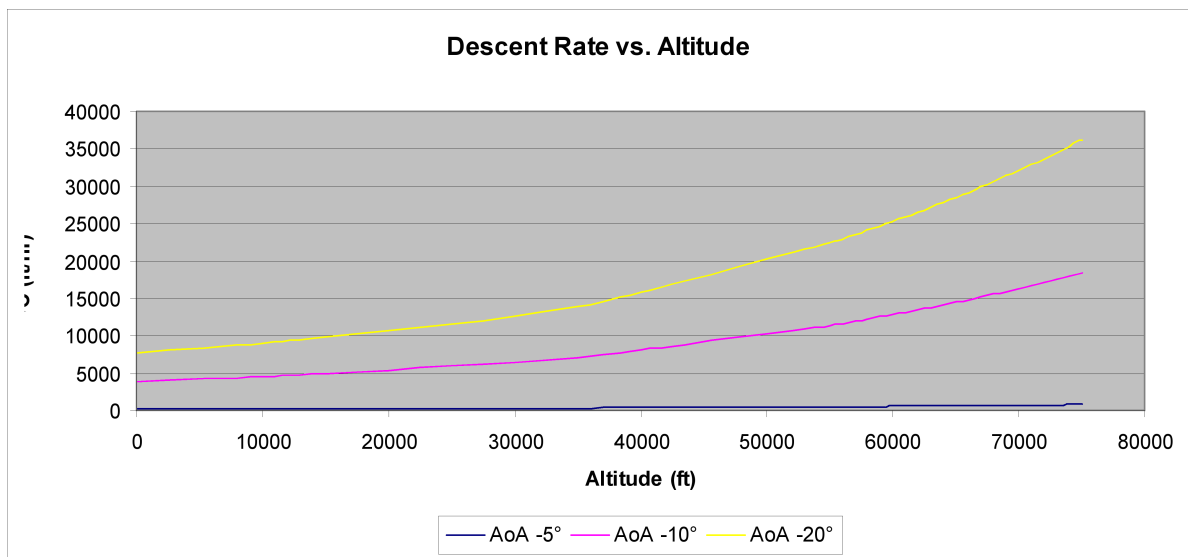


Figure 59: Descent Rate with Various Angles

12.3 Landing

Following the 720 hours of flight the SPACOM will be required to land; the distance required for landing can be found using,

$$S_L = \frac{1.69W^2}{g\rho_{\infty}SC_{L,\max}[D + \mu_r(W - L)]}$$

(20)

The distance required for the SPACOM to successfully land is approximately 760 ft, however since the break-away landing gear is not present it will require an assisted stopping mechanism, either by ground tethers or by hand.

12.4 Drag Polar

Since the SPACOM will be traveling at relatively lower speeds than conventional aircrafts it is important to minimize the overall drag as much as possible. Due to vast size most of the drag will be induced drag caused by the *wetted* surface area. This total area can be found using,

$$S_{wet} = 2S_{exp,ref} \{1 + 0.25(t/c)_r (1 + \tau\lambda) / (1 + \lambda)\}$$

(21)

The results for the total *wet* area are shown in Table 20

Table 20: Wetted Area

Area	S_{wet} (ft ²)
Wing/Fuselage	1,718
Horizontal	204
Vertical	61.2
Landing Gear	12.0
Total	1,995

Assuming a friction coefficient (C_f) of 0.007, this yields a parasite drag of approximately 0.012. The drag polars at various lift coefficients are shown below.

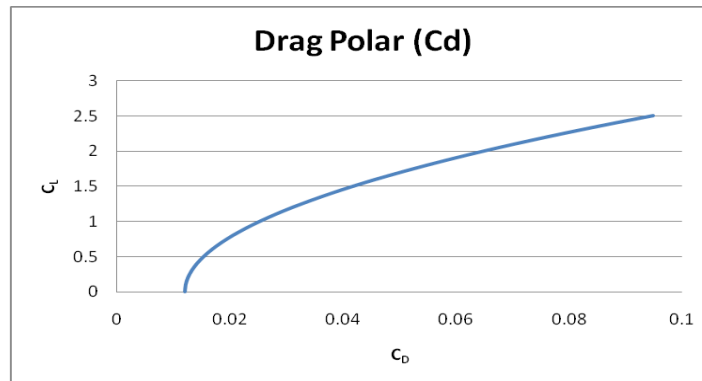


Figure 60: C_d vs C_L

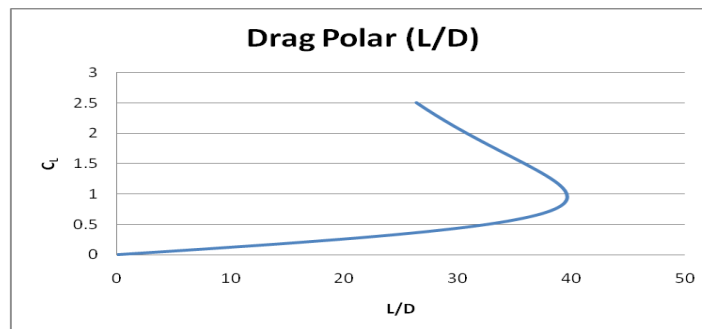


Figure 61: L/D vs C_L

As shown in Figure 61 at C_L of approximately 1.0 the total lift-to-drag ratio achieved is approximately 40, at cruise conditions. This is due to a lower C_L than previously assumed (1.0 instead of 1.5) and a lower value of induced drag (0.012 instead of 0.030). The value of induced drag is the actual result of the *wetted* body.

13.0 Conclusions

In conclusion, this study has summarized the history of solar flight, which included similar aircrafts which may be more than capable of meeting the minimum required mission specifications of this project. A comparison of various airfoils was conducted and it was found that there are various high lift / low drag airfoils which can be used for these types of aircrafts.

Next, a review of solar technology was conducted, and it was shown how much photovoltaic's have advanced throughout the years. It described how solar energy is affected by the atmosphere and how much solar radiation can actually be transferred to electrical energy. For this type of study, a solar cell with a high efficiency factor and low weight was found to be optimum.

Rechargeable batteries were considered to be used to power the SPACOM during night flight, however due to the weight constraints, $H_2 - O_2$ fuel cells were selected to power the aircraft at night. Research has shown that a typical fuel cell can possess an energy density of 0.230 kWh/lbs. Due to the high energy density the use of the fuel cells may generate enough power to keep the SPACOM aloft for longer than twelve hours of night flight.

After a comparison of various aircraft configurations was performed, it was found that the twin-boom configuration was the best fit for the SPACOM. The configurations were compared to the flying wing and the conventional configurations, due to the limitations in weight distribution. Since the SPACOM is similar to the *Helios* it was beneficial to observe the *Crash Incident Report* during the initial design phase.

This study has demonstrated that with the current and future technologies it is possible to design and build a HALE which is solely dependent on reusable energy, to stay aloft for 30+ days. The sole purpose of the SPACOM is to decrease the propagation between the war fighter and the communication beacon; this will allow continuous coverage over a specific region.

However, since most of this study took the most optimal solar radiation exposure, it would be feasible that the power requirements would increase substantially during winter, when solar radiation is at the minimum. Which would result in higher angles of attack to battle the high wind speeds.

The design of the study was based upon the required amount of solar energy required to power a HALE SPUAV for multiple days. This value (30 kW) over estimated the size of the SPACOM; upon completion of the power required calculations it is found that the SPACOM requires approximately 4.0 kW to maintain the cruising speed(s). If the SPACOM were to be resized according to the 4.0 kW requirements the total surface area would be 10% of what it is currently. The span would also be scaled down to approximately 30%.

The oversized wing area was found to be a critical flaw, since it is oversized. However, since the 100% of the surface area cannot be covered with solar cells, it may help when installing the rigid solar cells. There will be areas on the surface where the solar cells cannot cover, this can allow for more spacing if required.

In summary, there is no such thing as a free lunch; nor is there such thing as free energy. This study is direct proof of that. During the initial design, considerations were made to decrease the overall weight, which improved the performance. This yields that with the correct selection of components and materials; an aircraft like the SPACOM can be designed and built.

14.0 Recommendations / Lessons Learned

Should this study be continued by me or another individual, the following points should be taken into consideration:

- Energy is not free, even if it seems like it.
- Preliminary design shall be made based off lift-to-drag ratios, overall weight estimations, and/or stall speeds.
- The design did contain the actual amount of surface area which can be placed on the wing.
- Using literature and/or benchmark data from aircraft design's of conventional, military, and/or passenger uses does not useful 100% of the time.
- Conduct more thorough design reviews.
- Understanding & breakdown of communications hardware.
- Material selection & structural analysis can play a major role in the design.
- Scaled proto-type builds without fuel cells for aerodynamic testing purposes can assist in the design aspect; however will require much more time.
- Manufacturing the design can make design flaws more noticeable, rather than *building* on paper.

15.0 Design Summary

P_{total}/S	4.82 W/ft ²
P_{total}	3.93 kW
W	1,140 lbs
W/S	1.37 W/ft ²
W_{af}	300 lbs
W_{sc}	195 lbs
W_{fc}	450 lbs
S_w	830 ft ²
S_t	100 ft ²
b_w	160 ft
b_t	20 ft
c_{w0}	8.0 ft
c_t	5.0 ft
C_L	1.50
C_L/C_D	50.0
AR	30.0

Re	550,000
V_{cruise}	101 ft/s
Stall Angle of Wing	6.0°
V_{stream @ 90% of winds}	215 ft/s
R/C	137 ft/min
Fuel Cell Efficiency	50%
Solar Cell Efficiency	29%
Propeller Efficiency	80%
Design Altitude	65,000
Design latitude	33° N
Mission duration	30 days
Available solar radiation	125.80 W/ft ²
Atmosphere density	1.77 x 10 ⁻⁴ sl/ft ³
Configuration	Twin-boom, cantilever wings with single motor, two blade propeller blade (four total), two rudders, one elevator.

**Values are at maximum altitude of 65,000 feet.*

16.0 Reference List

1. Robert J. Boucher, *History of Solar Flight*. (1984).
<http://www.astroflight.com/pdfs/SolarHistory.pdf>. Accessed: 10 September 2010.
2. *The History of Solar*. U.S. Department of Energy: Energy Efficiency & Renewable Energy.
https://www1.eere.energy.gov/solar/pdfs/solar_timeline.pdf. Accessed: 16 September 2010.
3. Thomas E. Noll, John M. Brown, Marla E. Perez-Davis, Stephan D. Ishmael, Geary C. Tiffany, & Matthew Gaier, *Investigation of the Helios Prototype Aircraft Mishap*. (2004). Vol. 1.
http://www.nasa.gov/pdf/64317main_helios.pdf. Accessed: 14 September 2010.
4. Ed Wolski, "Unmanned Aircraft Systems," Department of Defense (DoD), Jan. 2009.
http://www.wired.com/images_blogs/dangerroom/files/Wolski.pdf. Accessed: 15 September 2010.
5. G. Palmisano, & R. Ciriminna, *Flexible Solar Cells*. (2008). Weinheim: Wiley-VCH.
6. J. Matthew Roney, "Solar Cell Production Climbs to Another Record in 2009," *Earth Policy Institute*. Sept. 2010.
<http://www.earthpolicy.org/index.php?/indicators/C47/>. Accessed: 23 September 2010.
7. Dryden Flight Research Center Fact Sheets. NASA.
<http://www.nasa.gov/centers/dryden/news/FactSheets/alphabetized.html>. Accessed: 5 October 2010.
8. *Breakthrough Unmanned Aerial Surveillance Technology*, Zephyr. Qinetiq. 2009.
<http://www.technologyshowcase.qinetiq.com/emag/Zephyr/index.html#/8/>. Accessed: 2 October 2010.
9. "Spies That Fly". PBS. NOVA Online. Nov. 2002.
<http://www.pbs.org/wgbh/nova/spiesfly/uavs.html>. Accessed Sept. 30 2010.

10. G. Warwick, & G. Norris. "Blue Sky Thinking: DARPA is 50 years old and still looking 20 years into the future," *Aviation Week and Space Technology*, pp. 2-6. Aug. 2008.
11. Amy Butler. "Global Hawk Operations". *Aviation Week and Space Technology*. pp. 36-37. Oct. 2007.
12. Brushless DC Electric Motor. Wikipedia: The Free Encyclopedia.
http://en.wikipedia.org/wiki/Brushless_DC_electric_motor.
Accessed: 24 Oct. 2010.
13. AID, Airfoil Investigation Database.
<http://www.worldofkrauss.com/>. Accessed 17 October 2010.
14. http://www.airfieldmodels.com/information_source/math_and_science_of_model_aircraft/formulas/straight_tapered_and_delta_wing_area.htm
15. D. Raymer. (1992), *Aircraft Design: A Conceptual Approach*. AIAA Education Series, Washington D.C., 1992.
16. M.D. Baily and M.V. Bower. *High Altitude Solar Power Platform*. NASA Technical Memorandum. 1992.
17. John D. Anderson. *Introduction to Flight*, 5th ed. McGraw-Hill Int. 2005.
18. John D. Anderson. *Fundamentals of Aerodynamics*, 4th ed. McGraw-Hill. 2004.
19. U.S. Centennial Flight Commission. *Wind Speed vs. Altitude*.
http://www.centennialofflight.gov/essay/Theories_of_Flight/atmosphere/TH1G3.htm. Accessed: 1 October 2010
20. Llyod R. Jenkinson, James F. Marchman III. *Aircraft Design Projects*. Butterworth Heinemann.
21. Noth, A. (2008), *Design of Solar Powered Airplanes for Continuous Flight* (Doctoral dissertation, ETH Zürich, 2008), ETH Zürich, Sept. 2008.
22. G. Romeo, G. Frulla. *Heliplat: Design of High Altitude very-long endurance solar powered platform for telecommunication and earth observation*. <http://adsabs.harvard.edu/full/2002ESASP.509E..54R>. Accessed: 02 November 2010.

23. Youngblood, J.W., and Jackson, R.D.: "Airborne Reconnaissance in the Civilian Sector: Agriculture Monitoring From High-Altitude Power Platforms." Society of Photo-Optical Instrumentation Engineers 27th Annual International Technical Symposium, August 21-26,
24. Spectrolabs Data Sheet. <http://www.spectrolab.com/>. Accessed 07 December 2010.
25. Dryden Flight Research Center. Helios Fact Sheet. http://www.nasa.gov/topics/technology/hydrogen/fc_shuttle.html. Accessed 02 December 2010.
26. Eye Lighting International of North America, Inc. "Solar Energy," Eye Lighting International of North America, Inc. Dec. 2008. <http://www.eyesolarlux.com/Solar-simulation-energy.htm>. Accessed: 17 November 2010.
27. Wikipedia. Solar Cell Technology. [http://en.wikipedia.org/wiki/File:PVEff\(rev100921\).jpg](http://en.wikipedia.org/wiki/File:PVEff(rev100921).jpg). Accessed: 15 January 2011.
28. Wikipedia. Fuel Cell. http://en.wikipedia.org/wiki/Fuel_cell. Accessed: 15 January 2011.
29. The Unitized Regenerative Fuel Cell. <https://www.llnl.gov/str/Mitlit.html>. Accessed: 10 January 2011.
30. Roskam, J. (1985-1990). *Airplane Design Part I-VIII*. Roskam Aviation and Engineering Corporation, Route 4, Box 274, Ottawa, Kansas
31. Stender, W.: "Sailplane Weight Estimation." OSTIV. June 1969.
32. XFLR5 v6.0. <http://xflr5.sourceforge.net/xflr5.htm>

PAGE INTENTIONALLY LEFT BLANK

Appendix A

Table 21: Raw Data with Respect to Altitude

Altitude (ft)	Density (slug/ft ³)	V (ft/s)	V (mph)	V _{stall} (ft/s)	L	D	T= D	L/ D	P (ft lbs/s)	P (watts)	R/C (ft/s)	R/C (ft/hr)	R/D (ft/s)
0	0.002377	27.7567 2	18.9250 4	24.0380 3	1140	22. 8		50	791.066 5	1072.97 4	2.41915 8	8708.96 7	0.04838 3
10,000	1.76E-03	32.2975 8	22.0210 8	27.9705 2	1140	22. 8		50	920.481	1248.50 7	2.81491 9	10133.7 1	0.05629 8
15,000	1.50E-03	34.9854 9	23.8537 4	30.2983 2	1140	22. 8		50	997.086 4	1352.41 2	3.04918 6	10977.0 7	0.06098 4
20,000	1.27E-03	38.0139 5	25.9186	32.9210 5	1140	22. 8		50	1083.39 8	1469.48 1	3.31313 4	11927.2 8	0.06626 3
25,000	1.07E-03	41.4422 2	28.2560 6	35.8900 2	1140	22. 8		50	1181.10 3	1602.00 6	3.61192 8	13002.9 4	0.07223 9
30,000	8.91E-04	45.3441 4	30.9164 6	39.2691 8	1140	22. 8		50	1292.30 8	1752.84	3.95200 2	14227.2 1	0.07904
35,000	7.38E-04	49.8076 1	33.9597 4	43.1346 6	1140	22. 8		50	1419.51 7	1925.38 1	4.34101 9	15627.6 7	0.08682
40,000	5.734E-04	56.5147 1	38.5327 5	48.9431 7	1140	22. 8		50	1610.66 9	2184.65 3	4.92558 1	17732.0 9	0.09851 2
55000	0.000286	80.0202 2	54.5592 4	69.2995 4	1140	22. 8		50	2280.57 6	3093.29 1	6.97422 2	25107.2	0.13948 4
55500	0.000279	81.0178 4	55.2394 3	70.1635 1	1140	22. 8		50	2309.00 8	3131.85 5	7.06117	25420.2 1	0.14122 3
56000	0.000273	81.9033	55.8431 6	70.9303 4	1140	22. 8		50	2334.24 4	3166.08 4	7.13834 3	25698.0 4	0.14276 7
56500	0.0002666	82.8805 6	56.5094 7	71.7766 7	1140	22. 8		50	2362.09 6	3203.86 1	7.22351 7	26004.6 6	0.14447
57000	0.0002603	83.8775 4	57.1892 3	72.6400 8	1140	22. 8		50	2390.51	3242.40 1	7.31040 9	26317.4 7	0.14620 8
57500	0.000254	84.9113 8	57.8941 2	73.5354 1	1140	22. 8		50	2419.97 4	3282.36 5	7.40051 4	26641.8 5	0.14801
58000	0.000248	85.9323	58.5902	74.4196	1140	22.		50	2449.07	3321.83	7.48950	26962.2	0.14979

		9	7	4		8			3	4	2	1	
58500	0.000242	86.9911 5	59.3121 5	75.3365 4	1140	22. 8		50	2479.24 8	3362.76 1	7.58177 8	27294.4	0.15163 6
59000	0.0002366	87.9782 6	59.9851 8	76.1914 1	1140	22. 8		50	2507.38	3400.92	7.66781 1	27604.1 2	0.15335 6
59500	0.000231	89.0382 8	60.7079 2	77.1094 1	1140	22. 8		50	2537.59 1	3441.89 6	7.76019 7	27936.7 1	0.15520 4
60000	0.000225	90.2176 5	61.5120 3	78.1307 7	1140	22. 8		50	2571.20 3	3487.48 6	7.86298 6	28306.7 5	0.15726
60500	0.00022	91.2370 9	62.2071 8	79.0136 3	1140	22. 8		50	2600.25 7	3526.89 4	7.95183 6	28626.6 1	0.15903 7
61000	0.000215	92.2918 9	62.9262 9	79.9271 2	1140	22. 8		50	2630.31 9	3567.66 9	8.04376 8	28957.5 6	0.16087 5
61500	0.00021	93.3841 4	63.671	80.8730 3	1140	22. 8		50	2661.44 8	3609.89 1	8.13896 4	29300.2 7	0.16277 9
62000	0.000205	94.5161 1	64.4428	81.8533 5	1140	22. 8		50	2693.70 9	3653.64 9	8.23762 1	29655.4 4	0.16475 2
62500	0.0002	95.6902 6	65.2433 6	82.8702	1140	22. 8		50	2727.17 3	3699.03 8	8.33995 6	30023.8 4	0.16679 9
63000	0.000195	96.9093	66.0745 2	83.9259 1	1140	22. 8		50	2761.91 5	3746.16 1	8.44620 2	30406.3 3	0.16892 4
63500	0.00019	98.1761 4	66.9382 8	85.0230 3	1140	22. 8		50	2798.02	3795.13 3	8.55661 4	30803.8 1	0.17113 2
64000	0.000186	99.2261 8	67.6542 1	85.9323 9	1140	22. 8		50	2827.94 6	3835.72 3	8.64813 1	31133.2 7	0.17296 3
64500	0.000181	100.587 4	68.5823	87.11122	1140	22. 8		50	2866.74	3888.34 2	8.76676 7	31560.3 6	0.17533 5
65000	0.000177	101.717 6	69.3529 1	88.0900 3	1140	22. 8		50	2898.95 2	3932.03 3	8.86527 3	31914.9 8	0.17730 5
65500	0.000173	102.886 8	70.1501	89.1025 9	1140	22. 8		50	2932.27 4	3977.23	8.96717 6	32281.8 3	0.17934 4
66000	0.000169	104.097 3	70.9754 2	90.1508 9	1140	22. 8		50	2966.77 3	4024.02 2	9.07267 6	32661.6 3	0.18145 4
66500	0.000165	105.351 5	71.8305 8	91.2370 9	1140	22. 8		50	3002.51 8	4072.50 6	9.18198 9	33055.1 6	0.18364
67000	0.000161	106.652	72.7174	92.3635	1140	22.		50	3039.58	4122.78	9.29535	33463.2	0.18590

		2	1	1		8			8	6	2	7	7
67500	0.000157	108.002 3	73.6379 2	93.5327 2	1140	22. 8		50	3078.06 5	4174.97 5	9.41301 9	33886.8 7	0.18826
68000	0.000153	109.405	74.5942 9	94.7474 8	1140	22. 8		50	3118.04 2	4229.19 8	9.53527 1	34326.9 8	0.19070 5
68500	0.00015	110.493 6	75.3365 4	95.6902 6	1140	22. 8		50	3149.06 8	4271.28 1	9.63015 2	34668.5 5	0.19260 3
69000	0.000146	111.997	76.3615 8	96.9922 3	1140	22. 8		50	3191.91 4	4329.39 6	9.76118	35140.2 5	0.19522 4
69500	0.000143	113.165 7	77.1584 2	98.0043 5	1140	22. 8		50	3225.22 2	4374.57 4	9.86303 9	35506.9 4	0.19726 1
70000	0.000139	114.782 4	78.2607 4	99.4044 8	1140	22. 8		50	3271.29 9	4437.07 1	10.0039 5	36014.2 1	0.20007 9
70500	0.000136	116.041 5	79.1192	100.494 9	1140	22. 8		50	3307.18 2	4485.74 2	10.1136 8	36409.2 6	0.20227 4
71000	0.000133	117.342 9	80.0065 4	101.622	1140	22. 8		50	3344.27 3	4536.05 1	10.2271 1	36817.6	0.20454 2
71500	0.00013	118.689 2	80.9244 3	102.787 8	1140	22. 8		50	3382.64 1	4588.09 1	10.3444 4	37239.9 9	0.20688 9
72000	0.000127	120.082 8	81.8746 5	103.994 8	1140	22. 8		50	3422.36	4641.96 5	10.4659 1	37677.2 7	0.20931 8
72500	0.000124	121.526 8	82.8591 5	105.245 3	1140	22. 8		50	3463.51 3	4697.78 2	10.5917 5	38130.3 2	0.21183 5
73000	0.000121	123.024 1	83.8800 4	106.542	1140	22. 8		50	3506.18 6	4755.66 3	10.7222 5	38600.1 1	0.21444 5
73500	0.000118	124.578 1	84.9396 2	107.887 8	1140	22. 8		50	3550.47 6	4815.73 7	10.8577	39087.7 1	0.21715 4
74000	0.000115	126.192 6	86.0404	109.286	1140	22. 8		50	3596.48 9	4878.14 6	10.9984 1	39594.2 7	0.21996 8
74500	0.000112	127.871 5	87.1851 1	110.74	1140	22. 8		50	3644.33 8	4943.04 7	11.1447 3	40121.0 5	0.22289 5
75000	0.00011	129.028 7	87.9741 3	111.7422	1140	22. 8		50	3677.31 9	4987.78 1	11.2455 9	40484.1 4	0.22491 2

Altitude	R/D	Total Night	R/D (ft/s)	R/D	Total Night	R/D (ft/s)	R/D	Total Night
----------	-----	-------------	------------	-----	-------------	------------	-----	-------------

(ft)	(ft/hr)	Decent		(ft/hr)	Decent		(ft/hr)	Decent
0	174.1793	2090.15218	0.09639808	347.0331	4164.39704	0.189867	683.5217	8202.260989
10,000	202.6742	2432.09039	0.11216831	403.8059	4845.67111	0.220928	795.3424	9544.108961
15,000	219.5414	2634.49679	0.12150332	437.412	5248.94346	0.239315	861.5334	10338.40044
20,000	238.5457	2862.54802	0.13202107	475.2759	5703.31033	0.260031	936.1107	11233.32845
25,000	260.0588	3120.70555	0.14392733	518.1384	6217.66066	0.283482	1020.533	12246.40084
30,000	284.5442	3414.52988	0.15747854	566.9228	6803.07312	0.310172	1116.62	13399.4383
35,000	312.5534	3750.64084	0.17298002	622.7281	7472.73704	0.340704	1226.535	14718.41874
40,000	354.6418	4255.70219	0.19627352	706.5847	8479.01591	0.386583	1391.7	16700.40121
55000	502.144	6025.72742	0.2779073	1000.466	12005.5954	0.547371	1970.534	23646.40689
55500	508.4042	6100.8507	0.281372	1012.939	12155.2702	0.554195	1995.101	23941.20874
56000	513.9607	6167.52864	0.28444719	1024.01	12288.1187	0.560252	2016.906	24202.86907
56500	520.0932	6241.11846	0.28784116	1036.228	12434.7382	0.566936	2040.971	24491.65326
57000	526.3494	6316.19333	0.29130363	1048.693	12584.3166	0.573756	2065.522	24786.26513
57500	532.837	6394.04429	0.29489412	1061.619	12739.426	0.580828	2090.981	25091.77108
58000	539.2441	6470.92935	0.29844007	1074.384	12892.611	0.587812	2116.124	25393.48658
58500	545.888	6550.65633	0.30211709	1087.622	13051.4582	0.595055	2142.196	25706.35448
59000	552.0824	6624.9885	0.3055453	1099.963	13199.5568	0.601807	2166.504	25998.0518
59500	558.7342	6704.81051	0.3092267	1113.216	13358.5934	0.609058	2192.608	26311.29264
60000	566.135	6793.61982	0.31332259	1127.961	13535.5361	0.617125	2221.65	26659.80177
60500	572.5322	6870.38632	0.31686308	1140.707	13688.4849	0.624098	2246.754	26961.05203
61000	579.1513	6949.81539	0.32052635	1153.895	13846.7385	0.631314	2272.729	27272.75085
61500	586.0054	7032.06459	0.3243197	1167.551	14010.6109	0.638785	2299.626	27595.51653
62000	593.1087	7117.30485	0.32825099	1181.704	14180.4427	0.646528	2327.502	27930.01985
62500	600.4768	7205.72197	0.3323288	1196.384	14356.604	0.65456	2356.416	28276.98992
63000	608.1265	7297.5183	0.33656246	1211.625	14539.4981	0.662899	2386.435	28637.22088
63500	616.0762	7392.91475	0.34096215	1227.464	14729.565	0.671564	2417.632	29011.57952
64000	622.6655	7471.9856	0.34460891	1240.592	14887.1049	0.678747	2443.489	29321.87262
64500	631.2072	7574.48677	0.34933628	1257.611	15091.3271	0.688058	2477.009	29724.11189
65000	638.2997	7659.59603	0.35326153	1271.741	15260.8979	0.695789	2504.842	30058.10116
65500	645.6367	7747.64026	0.35732214	1286.36	15436.3163	0.703787	2533.634	30403.60792
66000	653.2327	7838.7921	0.36152607	1301.494	15617.9263	0.712067	2563.442	30761.30973
66500	661.1032	7933.23879	0.36588196	1317.175	15806.1008	0.720647	2594.328	31131.94129

67000	669.2653	8031.18371	0.3703992	1333.437	16001.2453	0.729544	2626.358	31516.3008
67500	677.7374	8132.84831	0.37508798	1350.317	16203.8007	0.738779	2659.605	31915.2572
68000	686.5395	8238.47415	0.37995946	1367.854	16414.2485	0.748374	2694.147	32329.75843
68500	693.3709	8320.45103	0.38374024	1381.465	16577.5784	0.755821	2720.955	32651.45549
69000	702.805	8433.65965	0.38896144	1400.261	16803.1341	0.766104	2757.976	33095.7134
69500	710.1388	8521.66544	0.39302027	1414.873	16978.4759	0.774099	2786.756	33441.06933
70000	720.2841	8643.40969	0.39863513	1435.086	17221.0378	0.785158	2826.569	33918.82309
70500	728.1851	8738.2214	0.40300786	1450.828	17409.9397	0.793771	2857.574	34290.88713
71000	736.3519	8836.22321	0.40752772	1467.1	17605.1974	0.802673	2889.622	34675.46985
71500	744.7998	8937.59812	0.41220314	1483.931	17807.1757	0.811882	2922.774	35073.2894
72000	753.5453	9042.54416	0.41704327	1501.356	18016.2691	0.821415	2957.094	35485.12296
72500	762.6063	9151.27605	0.42205799	1519.409	18232.9054	0.831292	2992.651	35911.81311
73000	772.0023	9264.02703	0.42725808	1538.129	18457.5492	0.841534	3029.523	36354.27514
73500	781.7542	9381.05096	0.43265524	1557.559	18690.7064	0.852164	3067.792	36813.50524
74000	791.8854	9502.62472	0.43826224	1577.744	18932.9287	0.863208	3107.549	37290.59
74500	802.4209	9629.05101	0.44409304	1598.735	19184.8191	0.874693	3148.893	37786.71722
75000	809.6828	9716.19352	0.44811206	1613.203	19358.4409	0.882608	3177.39	38128.68543

Appendix B

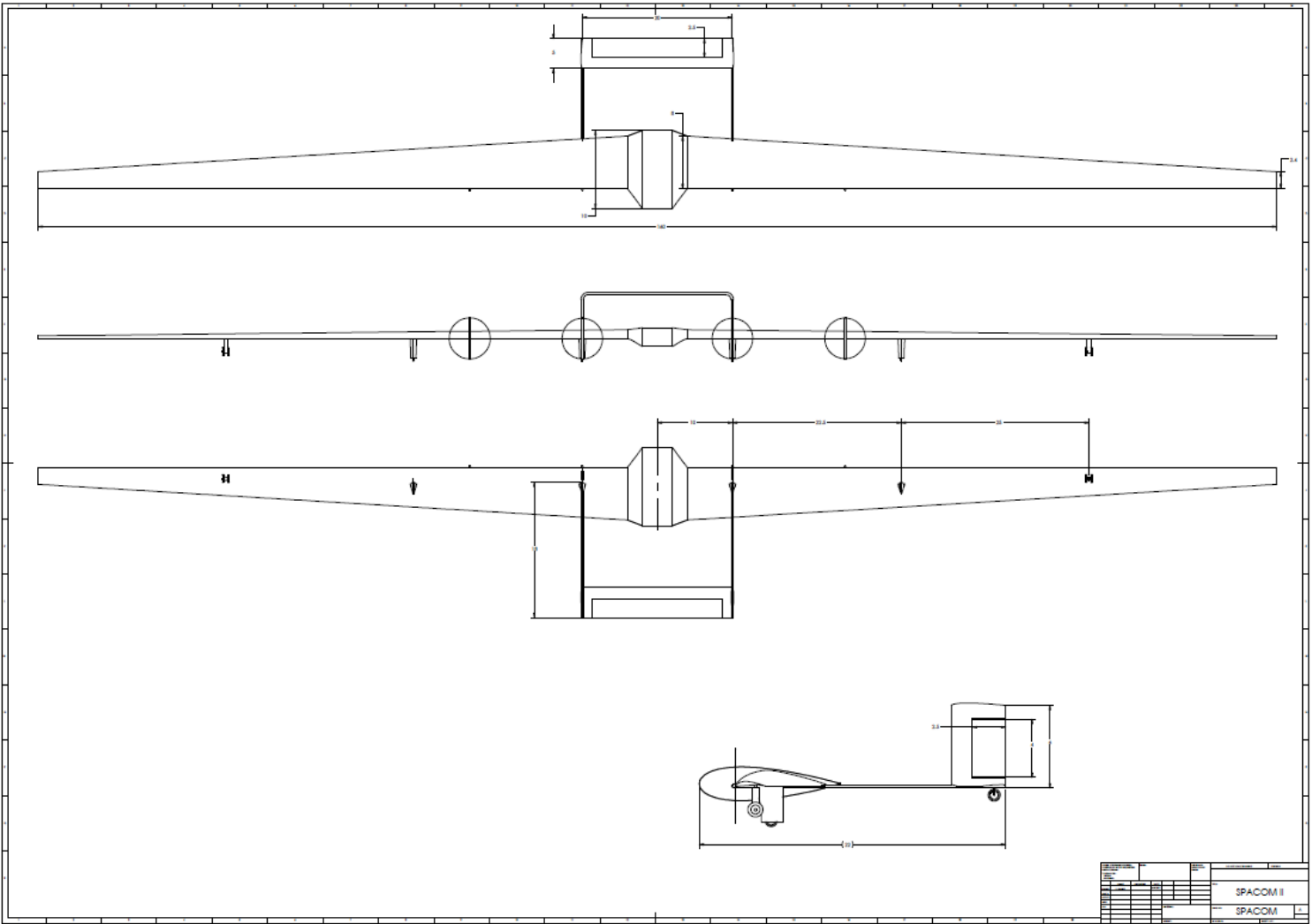


Figure 62: Final Design

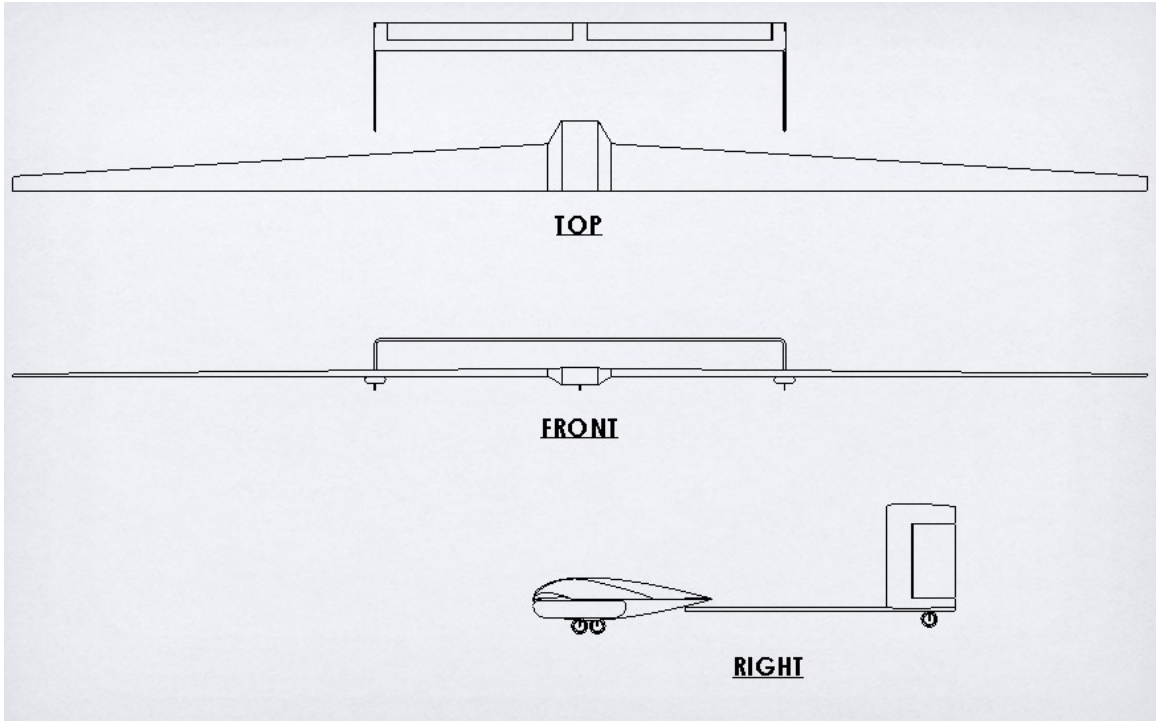


Figure 63: Initial Design with Low Gear

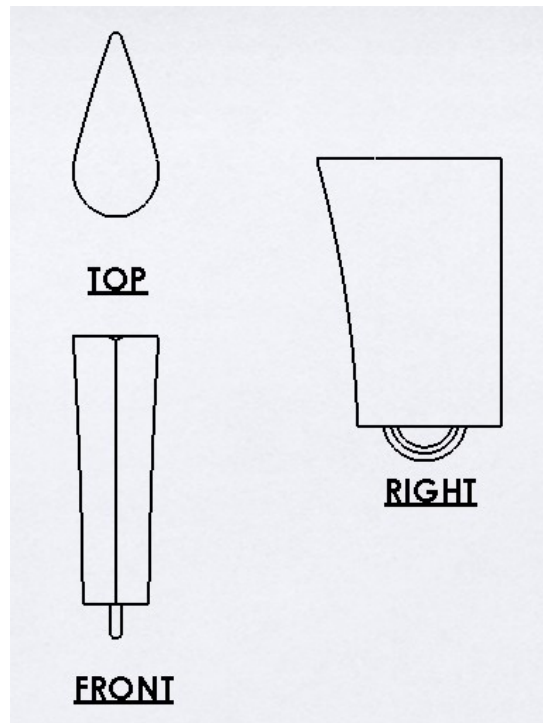


Figure 64: Landing Gear

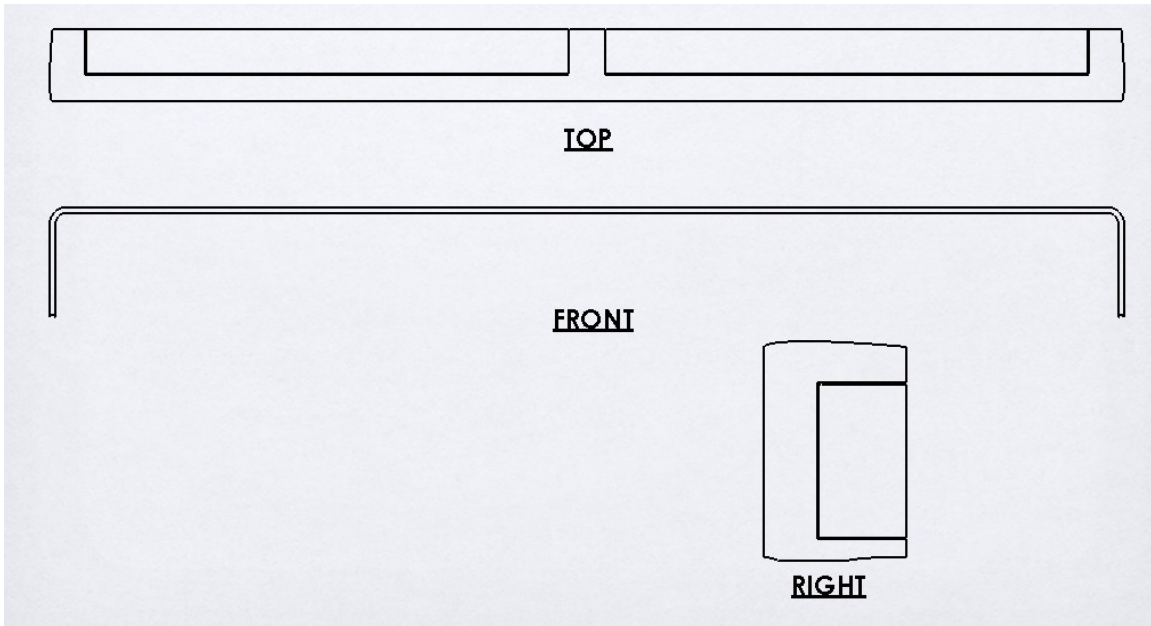


Figure 65: Tail Configuration